D1.4 -- Short Report on Models That Incorporate Non-stationary Time Variant Effects

Steinböck, Gerhard; Fleury, Bernard Henri; Lostanlen, Yves; Pedersen, Troels; Steinboeck, Gerhard; Stéphan, Julien; Wang, Wei

Publication date:
2011

Document Version
Early version, also known as pre-print

ICT–248894 WHERE2

D1.4

Short Report on Models That Incorporate Non-stationary Time Variant Effects

Contractual Date of Delivery to the CEC: M12
Actual Date of Delivery to the CEC: 11.07.2011
Editor: Gerhard Steinboeck, Bernard H. Fleury
Authors: Yves Lostanlen, Troels Pedersen, Gerhard Steinboeck, Julien Stéphan, Wei Wang
Participants: AAU, DLR, SIR
Work package: WP1 – Scenarios, Relevant Models and Market Feedback
Est. person months:
Security: PU
Nature: R
Version: 1.0
Total number of pages: 46

Abstract:

This deliverable summarizes the activities and achievements of investigations of WP1 Task 1.2 in the first year of the project. In the deliverable the research focus is on the non-stationary time variant effects of the radio channel.
Estimation results of time variant multipath parameters of outdoor-to-indoor environments are presented. Furthermore, the impact of human activity on the time variation of the radio channel is investigated and first simulation results are presented. Movement models, which include realistic interaction between nodes, are part of current research activities.

Keyword list: Multi-link channels, time-variant channels, non-stationary channels, human activity, mobility models, fingerprinting, positioning, tracking, non-line of sight bias, outdoor-to-indoor.

Disclaimer:

EXECUTIVE SUMMARY

This short report summarizes the ongoing activities of T1.2 in WHERE2 WP1 on the characterization, i.e., measurement, modeling and estimation of non-stationarity and time varying effects. This report is structured in two parts, a body part that provides a summary of the reported activities organized topic-wise, and an appendix containing all related publications and reports produced within WP1. The latter documents are meant to provide the readers with more detailed information on the activities if needed or wanted.

In Section 2 first results on the non-stationarity of the radio channel are summarized for scenarios with moving transmitter or receiver. A platform for measuring the time variant channel response is introduced. This platform allows for a high reproducibility of measurement locations and antenna orientations. Several conducted measurement campaigns made use of this platform. Research results on the time variation of multipath components for an outdoor-to-indoor environment are summarized. In the considered environment various transmitters (outdoors) and a moving receiver in an office building are located on different floors (heights). An algorithm for tracking multipath parameters is introduced for the estimation of time variant parameters. The algorithm is based on a combination of the Space-Alternating Generalized Expectation-maximization (SAGE) algorithm and the Kalman filter (KF). Detailed information on the algorithm and the results can be found in Appendices A.1, A.2 and A.3.

The research activities of non-stationarity due to human interaction are summarized in Section 3. The focus is put on three main activities: 1. modeling of human interaction in channel models, 2. movement models for human activity and 3. stochastic models for antenna responses and rotation due to human activity.

1. A new stochastic channel model is proposed for modeling the human interaction in channel models. The idea is to introduce time-variant components into a geometry-based stochastic channel prediction (i.e. WINNER 2). The model formulation is generic but it has been adjusted up to now, to static line-of-sight links within corporate environments. A detailed description of first results can be found in Appendix A.4.

2. Movement models in communications and localization are typically statistical models and interactions with other objects, such as walls or other agents, are modeled independently. In multi-link communication and localization the interaction between walls and agents is important. A survey of available models, which include more realistic interactions between nodes and the environment, is currently conducted and first findings are summarized.

3. The human interaction resulting in changed antenna responses and unknown terminal orientation has been identified as crucial for localization with fingerprints. Thus stochastic models, including the variation of the antenna response and terminal orientation, are necessary to obtain more robust localization systems, e.g., using fingerprinting.

Together with the results from D1.3 on the statistical dependency of multi-link channels and investigations with ray-tracing tools in D1.5 and D1.6, a description of a multi-link channel model for localization will be prepared and continuously shared with the other work packages in WHERE2.

TABLE OF CONTENTS

Authors

Partner	Name	Phone/e-mail
AAU	Bernard H. Fleury	Phone: +45 9940 8629 e-mail: bfl@es.aau.dk
	Troels Pedersen	Phone: +45 9940 8672 e-mail: troels@es.aau.dk
	Gerhard Steinboeck	Phone: +45 9940 8615 e-mail: gs@es.aau.dk
DLR	Ronald Raulefs	Phone: +49 8153 28 2803 e-mail: Ronald.Raulefs@dlr.de
	Wei Wang	Phone: +49 8153 28 2801 e-mail: Wei.Wang@dlr.de
SIR	Julien Stéphan	Phone: +44 223 480 500 e-mail: jstephan@siradel.com
	Yves Lostanlen	Phone: N/A e-mail: ylostanlen@siradel.com

List of Acronyms and Abbreviations

3GPP	3rd Generation Partnership Project
AoA	Azimuth of Arrival
BER	Bit Error Ratio
CIR	Channel Impulse Response
EKF	Extended Kalman Filter
GLoS	Geometrical Line-of-Sight
KF	Kalman Filter
LoS	Line-of-Sight
NLoS	None Line-of-Sight
SAGE	Space-Alternating Generalized Expectation-maximization
SISO	Single Input Single Output
TB	Time Based
RIMAX	Richter Maximization

1 INTRODUCTION

In this deliverable the intermediate research results, conducted in WHERE2 WP1, for the purpose of characterizing the non-stationarity of multi-link radio channels are presented. The time variation of the radio channel plays an important role in both radio communication and localization. The purpose of channel models for communications is the statistical evaluation of the performance of wireless communication systems. In indoor measurement campaigns for communication purposes, transmitter and receiver are typically moved by hand in an "uncontrolled" fashion. This results in unknown transmitter and receiver positions and as well unknown antenna orientations during the measurement. Human interaction is often conducted with people moving "randomly" (often unnatural) in the room. These circumstances render the measurements un-reproducible. For channel models used to statistically evaluate the performance of communication transceivers this is sufficient. In localization, however, exact information regarding the transmitter and receiver location, the antenna orientation and the human interaction is of crucial importance. Radio channel modeling in WHERE 2 focuses additionally on multi-link channels. As such the time variation of the channel needs to be determined and modeled for multiple links. Multi-link channel measurements are often conducted sequentially, by assuming the environment to be static for the measurement period. However, to conduct such measurements a high reproducibility of the transmitter and receiver trajectories need to be ensured.

In the following the intermediate research results, conducted in WHERE2 WP1, for the purpose of characterizing the non-stationary time variant effects for single- and multi-link radio channels, are presented. This report is structured in two parts, a body part that provides a summary of the reported activities organized topic-wise, and an appendix containing all related publications and reports produced within WP1. The latter documents are meant to provide the readers with more detailed information on the activities if needed or wanted.

Section 2: First results on the non-stationarity of the radio channel are presented. A platform for measuring the time variant channel response that results when the transmitter or the receiver is moving is introduced, which allows for a high reproducibility of measurement locations and antenna orientations. An algorithm for tracking multipath parameters, based on a combination of the Space-Alternating Generalized Expectation-maximization (SAGE) algorithm and the Kalman filter (KF), is used to estimate the time-varying channel model parameters for localization. First results obtained in the WHERE2 project on time variant parameters are presented.

Section 3: The research activities of non-stationarity due to human interaction are presented. A new stochastic channel model is proposed. The idea is to introduce time-variant components into a geometry-based stochastic channel prediction (i.e. WINNER 2). The model formulation is generic but has been adjusted up to now, to static line-of-sight links within corporate environments. Movement models in communications and localization are typically statistical models and interactions with other objects, such as walls or other agents, are modeled independently. In multi-link communication and localization the interaction between walls and agents is important. A survey of available models, which include more realistic interaction between nodes and the environment, is currently conducted and first findings are summarized. Furthermore the human interaction resulting in changed antenna responses and unknown terminal orientation has been identified as crucial for localization with fingerprints. Thus stochastic models, including the variation of the antenna response and terminal orientation, are necessary to obtain more robust localization systems, e.g., using fingerprinting.

Section 4: Conclusions.

Appendix A: The appendix contains a collection of already/soon to be published articles or reports from the WHERE2 project. This collection contains detailed information to the various sections in the deliverable.

2 NON-STATIONARY TIME VARIANT CHANNEL

Models of the radio channel are an essential tool for receiver development in terms of localization in communication networks. Due to a dissimilar focus between communication and positioning, requirements to channel models for these applications differ.

- For communications in mobile radio networks, multipath modeling is more used to evaluate the Bit Error Rate (BER), and is considered as the most essential criterion for algorithms evaluation, like channel estimation, coding/decoding, and synchronization.
- Localization using mobile radio networks focuses on investigating of the position error, which is directly related to the range error of individual links. Two different major channel characteristics effect the range error. Firstly, the ranging based on the first detectable wave is positively biased if the Geometrical Line-of-Sight (GLoS) path is blocked. Generally this bias, between the geometrical distance from the transmitter to the receiver and the propagation distance of the first detectable path is known as the Non Line-of-Sight (NLoS) error [1]. Secondly due to multipath the correlator based synchronizer which is generally used for range estimation is biased [2].

In realistic scenarios for location-tracking/navigation applications, the multipaths are time-variant in delays, amplitudes, phases and incoming angles due to movements of transmitters, receivers, and/or reflectors. This results into the requirement of using channel models capable to reproduce propagation paths with delays in sub-sample domain and second having a smooth time evolution of the Channel-Impulse-Response (CIR) in the simulation process. Therefore, propagation paths within the CIR should be modeled having a continuous delay and a life-time or life-distance.

2.1 Measurement Platform for the Time-variant Wireless Channel

The absolute delay information of signal arrivals is essential in channel modeling for positioning applications [1]. Ranging based on the first detectable propagation path is positively biased if the LoS is blocked. This bias, i.e. the difference between the geometrical distance from the transmitter to the receiver and the propagation distance of the first detectable path is known as the Non Line-of-Sight (NLoS) bias. In order to obtain the necessary statistics a well located moving platform is needed in the measurement process. We propose a low-cost mobile measurement platform jointly fulfilling the requirements given by the positioning application. Accurate positioning of transmitter and receiver antennas is possible. The parameter space of the estimated CIR can be increased by the azimuth of arrival (AoA) due to the movement of the platform. Therefore, for measurements with a single receive or transmit antenna, the one dimensional AoA can be estimated.

A single antenna can be mounted on the experimental mobile platform realized by a model railway running on a cogwheel to prevent wheel slipping. A rotary encoder mounted on the motor allows determining the number of impulses per meter. Taking multiple measurements over accurately measured distances allows for determining the mean error $\mu = -2.4\,\mu\mathrm{m}/\mathrm{m}$ with standard deviation $\sigma = 0.23\,\mathrm{mm}/\mathrm{m}$ of the platform. By storing the number of rotary encoder impulses synchronously with each measured CIR snapshot, since the start of the train movement, a traveled distance for each CIR snapshot can be obtained in a straightforward manner. This platform can be used either at transmitter or receiver side. A more detailed explanation of the platform can be found in the measurement report in the appendix of the WHERE2 deliverable D1.3. The measurement jointly done by DLR and AAU described in WHERE2 deliverable D1.3 and some of the measurements used in this deliverable were performed with this platform.

In general, a measurement requiring a time-variant transceiver location information can gain benefits from the proposed platform with low-cost. Moreover, it is worth to mention that due to the accuracy of the platform, it is possible to generate a virtual antenna array based on the predicted traveled distance. Some measurement results based on this platform are presented in this deliverable in Section A.2 and Section A.3 .

2.2 Estimation of Time-variant Channel Parameters

Estimation of time-variant multipath parameters from channel measurement data is usually based on an underlying snapshot based estimator like the Space-Alternating Generalized Expectation-maximization (SAGE) algorithm [4] or RIMAX [5] and an attached path detection scheme as in [6]. Snapshot based algorithms do not consider the previous or consequent time information and are therefore non-optimal. With the fact that the multipath parameters vary slowly in time, some alternative algorithms have been proposed by utilizing a variable state dimension Extended Kalman Filter (EKF) to track propagation path parameters [7]. However, applying the EKF inherently means using a first order polynomial approximation, which is inadequate in scenarios where closed space multipath components are present. In such a situation the filter might lose its lock on tracking the global a-posteriori maximum and tracks local maxima or diverges completely. In Appendices A.1 and A.2 we propose a SAGE based Kalman Filter (KF) method to estimate and track the multipath components based on measurement data. Parallel Kalman filters are used to track the multipath components for a different number of paths. Instead of considering the measurement CIR directly in the Kalman filter as in [7], the estimator outcomes from SAGE are utilized. An information criterion based selection metric is used to select the most correct number of paths among the parallel Kalman filters. Some estimation results based on outdoor to indoor measurements are presented in Appendix A.2 in terms of path life, NLoS bias and its spatial characteristics. These estimated parameters can be used for further channel model parametrization or directly for localization algorithm testing. For instance, the NLoS bias obtained in the specified scenario could be modeled by an exponential distribution. It impacts the positioning algorithm performance due to different NLoS bias statistic assumptions. Meanwhile, the statistics of path life seem to follow a log-normal distribution. In order to check the time-variant characteristics in cooperative scenarios, it is worth to modify and apply the SAGE based KF algorithm to the channel data, measured jointly by DLR and AAU.

3 MODELING OF HUMAN MOBILITY

The human mobility plays an important role on the time variation of the radio channel. Radio channel models often consider only movement of transmitter or receiver entities. Thus the time variation of the radio channel is modeled based on this movement. For static transmitters and receivers the activities of humans, present in the environment, lead to strong variations in the radio channel as well. Section 3.1 proposes a model to deal with the effects of time-variation due to human mobility.

Typically statistical movement models are used in communication and localization. In these models interaction with other objects, such as walls or other agents, is modeled independently. More realistic movement models, considered in Section 3.2, include the interaction between walls and agents. This is important in models for multi-link communication and localization.

Furthermore the effect of human activity on the transmitter or receiver itself, for instance the impact on the antenna response or orientation of the antenna, plays a vital role in localization with fingerprints, as described in Section 3.3.

3.1 Introduction of a Time-variant Component Related to Human Activity Into WINNER 2 Model

It was proven that the human activity, i.e. location and movement of persons, has significant impacts on the wireless channel properties in indoor environments. Thus, these impacts need to be considered in realistic positioning approach. In Appendix A.4, we propose a new stochastic channel model simulating indoor time-variant channel properties related to human activity. The approach basically consists in introducing a time-variant contribution into a geometry-based stochastic channel prediction (WINNER 2), taking into account the path geometries and the random distribution of human bodies. The proposed solution is compatible with any kind of human activity properties, in terms of density or mobility. However it has been adjusted up to now for only a small number of human obstructions.

This time-variant channel model currently predicts multi-path channel properties for a static SISO radio link that undergoes variations due to human body obstructions. Using the WINNER 2 model, the exact trajectory of indirect paths (i.e. paths that undergo at least one interaction with the environment) is unknown. Then, for the first snapshot, simulation of obstruction of each indirect path by the person is determined randomly by an obstruction probability function. For the following snapshots, each probability that a person obstructs an indirect path is obtained by probability function depending on the previous obstruction state and state duration. The LOS direct path is distinguishable as its trajectory is fully known. Then the simulation of its "obstruction state", and even the prediction of the obstruction loss, may be done in a deterministic way. A new method was developed, inspired from [9] with some enhancements that permit to deal with a larger number of person distribution cases (especially when nobody obstructs the direct path) and to determine a Doppler shift. This method is still under investigation as the algorithm becomes more complex when several persons are in the vicinity of the LOS direct path. However, first simulation results are very close to observations and simulations reported in the literature.

As previously introduced, parameterization of this stochastic time-variant channel model relies on an obstruction probability function and an obstruction transition probability function, which have to be as close as possible to reality. We are currently studying the possibility to get these probability functions for a wide range of configurations from simulations, based on the realistic prediction of the channel multi-paths provided by the ray-tracing technique. Besides, the analysis of transition probabilities is not achieved, in the sense that we did not evaluate the duration of the obstruction state as a function of all geometrical parameters. The

proposed model should also be adapted in order to simulate the impact of groups of persons in busy areas, e.g. dense crowd effects in a shopping mall. Current modeling of shadowing loss and Doppler shift are notably expected to be not suitable. A measurement campaign is being specified in order to characterize simple radio link with controlled human activity.

3.2 Agent Based Mobility Models for Cooperative Communication and Localization in Indoor Scenarios

Models for terminal mobility are at interest for localization and communication in several ways at various layers of radio communication or localization systems. It is particularly relevant to design and simulation of multi-link systems, where the mobility imposes dependencies in between different communication links. Therefore mobility models have potential applications on both communication and localization.

Mobility models can be constructed assuming the movements of different nodes to be independent [10]. This approach may be feasible in situations where a low node density is considered. However, to realistically model systems in environments with high node density, the inter-node dependencies must be accounted for. Such scenarios include pedestrian mobility in shopping malls, train stations, airports, hospitals, etc. So-called agent based mobility models are used in other engineering fields such as fire evacuation simulation or pedestrian modeling for traffic evaluation [11, 12]. These models rely on the concept of individual agents (humans) which during their movement interact with other agents or e.g. walls by direct (contact) forces or indirectly due to social forces [11, 13]. Inspired by these approaches, an agent could in the setting of localization and communication represent a network node. One virtue of the agent based approach for indoor mobility modeling is that it inherently accounts for the constraints of the trajectory imposed by the building geometry.

There are several open issues to consider regarding agent based mobility models for indoor localization and communications. The available models are originally constructed for Monte Carlo simulation of pedestrian flows and are thus not directly applicable for modeling of node mobility. For localization, in particular, the models should be modified to allow for a solution of the inverse problem, e.g. to infer, based on noisy range estimates, on the trajectory of an agent using statistical estimation techniques. It is also an open issue to clarify which effects should be considered in agent based mobility models to reliably model node mobility in indoor localization and communication.

3.3 Impact of the Antenna Response and Terminal Orientation on Fingerprints

In fingerprinting, the position is found by comparing an observed fingerprint with fingerprints in a prerecorded database. The fingerprints can consist of measurements of parameters of the received signal at a specified position. Obviously, the precision of the method depends on the precision of the database. In general, one cannot assume, that the database is recorded with exactly the same equipment as the equipment used for the positioning. Thus, to evaluate the performance of such positioning algorithms it is of great importance to evaluate the effect of such uncertainties inherent in the fingerprints in the database.

The observed signal, and thus the matching of fingerprints, are affected by the antenna systems used to record the database and to record new fingerprints at the terminal to be localized. As a result, the observed signal may differ from the fingerprints in the database, even when the terminal is located at exactly the same position as used in the database. Moreover, this difference is affected by an unknown antenna response due to user operation, along with an unknown antenna orientation due to user movement.

To study the effect of the unknown and varying antenna response, along with the unknown, and possibly time-varying antenna orientation, it is necessary to propose stochastic

models including these effects. Thus mobility models accounting for the terminal orientation and stochastic models for the terminal antennas are needed. The statement and validation of such models are currently open issues. Once such models are available, the effect on a specific channel feature can be evaluated analytically or via computer simulations. The availability of such models will also improve the realism of Monte Carlo simulations of cooperative localization schemes, as effects due to the unknown antenna response and orientation can be taken into account.

4 CONCLUSIONS

This intermediate deliverable summarizes the ongoing activities of T1.2 in WHERE2 WP1 on the characterization, i.e., measurement, modeling and estimation of non-stationarity and time varying effects.

Research results on the time variation of multipath components for an outdoor-to-indoor environment were presented. The environment considered various transmitter positions and a moving receiver on different heights (floors) of an office building. Current investigations on the time variability due to human mobility complete this research topic. Human mobility creates, for instance due to blockage of multipath components, strong variations in the channel characteristics. A method has been proposed to introduce indoor time-variant channel properties related to human activity into a geometry-based stochastic channel model (i.e. WINNER2). Research on more realistic agent based movement models, as for instance for crowds, has been started. These movement models will become more important in radio channel modeling for localization and can be further utilized in positioning and tracking algorithms. The impact of the human mobility on fingerprinting, due to changed antenna responses and random antenna orientations, is a possible topic of future investigations. A stochastic model for the human activity, including these effects on the terminal, could improve the robustness of fingerprinting.

Together with the results from D1.3 on the statistical dependency of multi-link channels and investigations with ray-tracing tools in D1.5 and D1.6, a description of a multi-link channel model for localization will be prepared and continuously shared with the other work packages in WHERE2.

A APPENDIX

The appendix contains a collection of articles and reports with detailed information to the summaries of the different sections in this deliverable, which are results of the WHERE2 project. Table 1 lists titles of the following sections in the appendix.

Table 1: Overview of the collection of papers and reports.

A.1 Evaluation of Time-Variant Multipath Characteristics for Localization Channel Model in Terrestrial Mobile Radio

W. Wang and T. Jost. Evaluation of time-variant multipath characteristics for localization channel model in terrestrial mobile radio. In *COST Action IC0802, Propagation tools and data for integrated Telecommunication, Navigation and Earth Observation systems. MCM 3*, Athens, Greece, April 2010.

COST Action IC0802
Propagation tools and data
for integrated Telecommunication, Navigation and
Earth Observation systems

MCM 3: 26-28 April 2010
NTUA, Athens, Greece

Evaluation of Time-Variant Multipath Characteristics for Localization Channel Model in Terrestrial Mobile Radio

Wei Wang[(1)] and Thomas Jost[(1)]

[(1)] German Aerospace Center (DLR)
Institute of Communications and Navigation
82234 Wessling, Germany
Email: <first name>.<family name>@dlr.de

INTRODUCTION

Positioning by using Global Navigation Satellite Systems (GNSSs), such as the Global Positioning System (GPS) operating at L-band, promises very accurate location information, when a Line-of-Sight (LoS) condition to the satellite is present. However, positioning in urban canyons, where LoS might be absent, GNSSs do not provide accurate positions. For some indoor areas, like rooms with metallised windows, satellite signals can not be tracked by GPS receivers because of low signal power. Time Based (TB) localization, utilizing available ground communication networks [1][2], are investigated as a complementation to GNSS with the advantage of higher power level in comparison. By suitable Hybrid Data Fusion (HDF) algorithms to combine measures obtained from GNSS and terrestrial networks, the accuracy of the estimated position can be improved.

As an essential tool for receiver development in terms of TB localization in communication networks, wireless channel modelling has a growing significance. Due to a dissimilar focus between communications and positioning, channel models for both applications are different.

- For communications in mobile radio networks, multipath modelling is more used to evaluate the Bit Error Rate (BER) [3], and is considered as the most essential part for algorithms evaluation, like the channel estimation, coding/decoding, and synchronization.
- TB positioning using mobile radio networks focuses on investigating of the position error, which is directly related to the range error of individual links. Two different major channel characteristics affect the range error. Firstly, the ranging based on the first detectable wave is positively biased if the Geometrical Line-of-Sight (GLoS) path is blocked. Generally this bias, between the geometrical distance from the transmitter to the receiver and the propagation distance of the first detectable path is known as the Non Line-of-Sight (NLoS) error [4][5]. Secondly due to multipath the correlator based synchronizer which is generally used for range estimation is biased positively or negatively by the superposition of paths [2]. Besides, at least 3 transmitters with known positions are required to be linked to receiver for positioning. It is also important to evaluate the inter-link correlations of NLoS error for channel modelling.

In realistic scenarios for location-tracking/navigation applications, the multipath components are time-variant in delays, amplitudes, phases and incoming angles due to movements of transmitters, receivers, and/or reflectors. Therefore, it is essential to model the time evolution for each path as well as its life-time. Estimation of time-variant multipath parameters from channel measurement data is usually based on an underlying snapshot based estimator like the Space-Alternating Generalized Expectation-maximization (SAGE) algorithm [6] or RIMAX [7] and an attached path detection scheme as in [8]. Snapshot based algorithms do not consider the previous or consequent channel snapshot information and are therefore non-optimal. With the fact that the multipath parameters vary slowly in time, some alternative algorithms have been proposed by utilizing a variable state dimension Extended Kalman Filter (EKF) to track propagation paths parameters [9]. However, applying the EKF inherently means using a first order polynomial approximation, which is inadequate in scenarios where closed space multipath is present. In such a situation the filter might loose its lock on tracking the global a-posteriori maximum and track local maxima or disconverges completely. In this paper, we utilize a SAGE based Kalman Filter (KF) method to estimate and track the multipath based on a

dynamic Single Input Single Output (SISO) measurement. 1-D Angle of Arrival (AoA) information is used by utilizing a Virtual Antenna Array (VAA) in post-processing.

CHANNEL MEASUREMENT CAMPAIGN

The measurement was accomplished in the SISO manner with a MEDAV RUSK broadband channel sounder at premises of the German Aerospace Center (DLR). A spread signal --- in particular an Orthogonal Frequency Division Multiplexing (OFDM) signal --- has been sent by the transmitter. The parameter setup of the channel sounder is summarized in **Error! Not a valid bookmark self-reference.**. The measured i-th snapshot of the Channel Impulse Response (CIR), $h(i,j)$, $j=0,\ldots,M-1$ consists of M = 1537 samples at delays $\tau_j=j\Delta\tau$, with $\Delta\tau=1/B$, with a bandwidth of $B=120$ MHz The channel sounder records one CIR every T_g = 1.024 ms providing a measurement rate of 976 CIRs per second (CIRs/s).

Table 1: Channel sounder settings for the measurement

RF Center Frequency	5.2 GHz
Bandwidth	B= 120 MHz
Transmitted Power	5W
Signal Period	12.8 µs
Measurement Time Grid	1.024 ms
Antennas	Omni-directional (V-poliraized)
Receiver Speed	$v \approx 0.15$ m/s

The measurement was performed on the second floor (~9 m above ground) of the building characterized as a standard three story office building of concrete with non-metallic window glass as described in [10]. In order to perform a dynamic measurement, the receiving antenna was mounted on a model train running along two tracks *R1* and *R2* planted on the ground with a speed of $v \approx 0.15$ m/s, where no LoS is present as displayed in Figure 1. The transmitter was positioned above the points Tx-1 and Tx-2 as shown in Figure 1 in heights of $H1=12$ m and $H2=18$ m. Hence, overall four different transmitter positions were achieved.

The position of the transmitter was precisely determined using a Leica tachymeter giving a nominal accuracy in the sub-cm domain. To get a similar accuracy for the receiver antenna mounted on the model train, the train is equipped with a rotary encoder giving 500 impulses per motor turn as described in [10]. To prevent wheel slipping the model train runs by a cogwheel. Together with each CIR snapshot measurement $h(i,j)$ the number of impulses given by the rotary encoder, since the model train started to move, is saved, which results in a precise travelled distance measure for each captured impulse response snapshot. To validate the accuracy of the distance measurement by rotary encoder, $k=1,\ldots,K$, with $K=21$ train runs have been performed. The K distance errors between estimated travelled distances d_k^{est} and the real distances d_k have a mean value of 0.16 mm/m and a standard deviation of 0.14 mm/m. As the time of arrival is the most important value for navigation receivers and therefore the most important part in this measurement campaign, receiver and transmitter were perfectly synchronized by cable connection using one common rubidium atomic clock serving as frequency normal. This setup prevents time drifts which usually occur in channel sounder measurements using separated clocks.

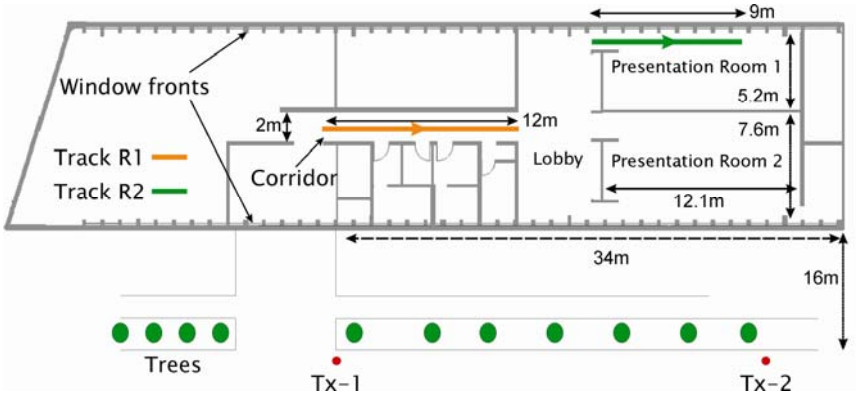

Figure 1: Building layout with track *R1* and *R2*. Tx-1 and Tx-2 indicate azimuth positions of the transmtiter. All rooms are lcoated on the high-level of the building, which is ~ 9 m above the ground.

Generally, estimation of AoA information with an antenna array is performed by taking incoming phase differences of different antenna elements into account. As described in above, the measurement was performed in the SISO manner with a single antenna which does not provide spatial phase difference information. However, it is possible to extract a

linear antenna array from the measurement due to the utilization of the rotary encoder. The distance error per meter estimated through the odometer measurement is 0.16 mm/m in average, which is small enough to be ignored. As a result, it is possible to form a uniform linear VAA with element-spacing *d* as shown in Figure 2. In this paper, the train movement direction is defined as the travelling direction, meaning that for the receiver antenna positioned at the end of the track a ray coming from the start point of the track has an AoA of 0°. The receiver was running from the left to the right for tracks *R1* and *R2* as depicted in Figure 1. A VAA snapshot is defined as $\boldsymbol{h}(i)=[\bar{h}(i),\ldots,\bar{h}(i+(N_E-1)\cdot d)]^T$, where $(\bullet)^T$ stands for vector or matrix transpose, N_E is the number of elements, and $\bar{h}(i)$ stands for the measured CIR at time i as a column vector. For each VAA snapshot, the Fourier transform of CIRs $\boldsymbol{h}(i)$ for each row is denoted as $\boldsymbol{H}(i)$. More details on the VAA and SAGE processing can be found in [4].

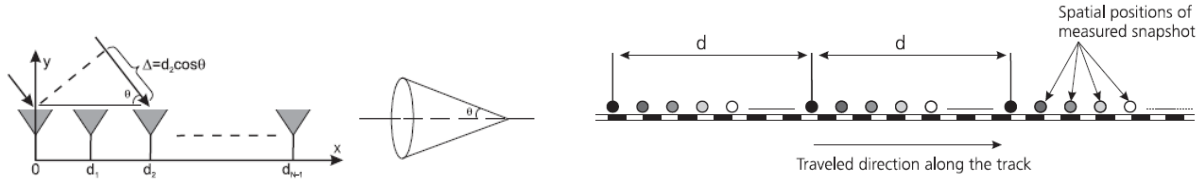

Figure 2: VAA generation from the measurement

SAGE BASED KF METHOD FOR MULTIPATH ESTIMATION AND TRACKING

The purpose of the method described here, is to track the parameter vector $\boldsymbol{\theta}_l(i)=[\alpha_l(i),\nu_l(i),\tau_l(i),\Delta\alpha_l(i),\Delta\nu_l(i),\Delta\tau_l(i)]^T$, for each path l, with $l=1,\ldots,N(i)$. The elements of $\boldsymbol{\theta}_l(i)$ are the complex amplitude $\alpha_l(i)$, its AoA $\nu_l(i)$, its delay $\tau_l(i)$ as well as the rates $\Delta\alpha_l(i)$, $\Delta\nu_l(i)$, and $\Delta\tau_l(i)$. The state vector $\Theta(i)$ of the KF describes the states for all paths as $\Theta(i)=[\boldsymbol{\theta}_1(i)^T,\ldots,\boldsymbol{\theta}_{N(i)}(i)^T]^T$. Instead of taking directly $\boldsymbol{H}(i)$ as measurement into the tracking filter as done in [9], a maximum search converging to the next maximum of the likelihood function around the prediction $\hat{\Theta}^-(i)$ is used. This yields a faster convergence of the tracking filter over time i as well as a more robust behavior.

For the maximum likelihood search, the SAGE algorithm [6] is favored denoted by $S\left[\boldsymbol{H}(i),\hat{\Theta}^-(i)\right]$ starting at the predicted value $\hat{\Theta}^-(i)$. The Kalman filter as the outer estimator is defined by

$$\begin{aligned}
\hat{\Theta}^-(i) &= \boldsymbol{F}\cdot\hat{\Theta}(i-1)\\
\hat{\boldsymbol{P}}^-(i) &= \boldsymbol{F}\cdot\hat{\boldsymbol{P}}(i-1)\cdot\boldsymbol{F}^H+\boldsymbol{W}\\
\boldsymbol{K} &= \hat{\boldsymbol{P}}^-(i)\cdot\Gamma^H\cdot\left[\Gamma\cdot\hat{\boldsymbol{P}}^-(i)\cdot\Gamma^H+\boldsymbol{R}\right]\\
\hat{\Theta}(i) &= \hat{\Theta}^-(i)+\boldsymbol{K}\cdot\left[S\left[\boldsymbol{H}(i),\hat{\Theta}^-(i)\right]-\Gamma\cdot\hat{\Theta}^-(i)\right]\\
\hat{\boldsymbol{P}}(i) &= \left(\boldsymbol{I}-\boldsymbol{K}\cdot\Gamma\right)\cdot\hat{\boldsymbol{P}}^-(i)
\end{aligned} \tag{1}$$

where Γ represents a simple mapping matrix between the state vector $\hat{\Theta}^-(i)$ and the values calculated in the SAGE algorithm. $\boldsymbol{F}$ represents the state transition matrix in the system equation, $\boldsymbol{W}$ the covariance of the process noise, $\boldsymbol{K}$ the Kalman gain matrix and $\boldsymbol{R}$ the covariance of the measurement noise.

Figure 3 displays the overall routine including the model order selection part. From the last time step $i-1$ the model order $N(i-1)$, $\Delta(i-1)$ and the tracking results $\hat{\Theta}(i-1)$ and $\hat{\boldsymbol{P}}(i-1)$ are used. $\Delta(i)$ represents an additive factor to the model order selection criteria based on each snapshot as shown in Figure 3. For model order selection the Minimum Description Length (MDL) [11], using the sample covariance matrix for decreasing the computational complexity, is utilised.

After calculating the new model order at time i, $\hat{N}(i)$, several tracking filters (denoted in Figure 3 only as KALMAN) are running in parallel each with a different model order around the estimated $\hat{N}(i)$.

- If the model order set to a tracking filter is larger than $N(i-1)$, new paths are initialised by calculating the residual sequence

$$\boldsymbol{Res}\left(i \mid \hat{\Theta}(i-1)\right) = \boldsymbol{H}(i) - \boldsymbol{H}\left(i \mid \hat{\Theta}(i-1), N(i-1)\right) \tag{2}$$

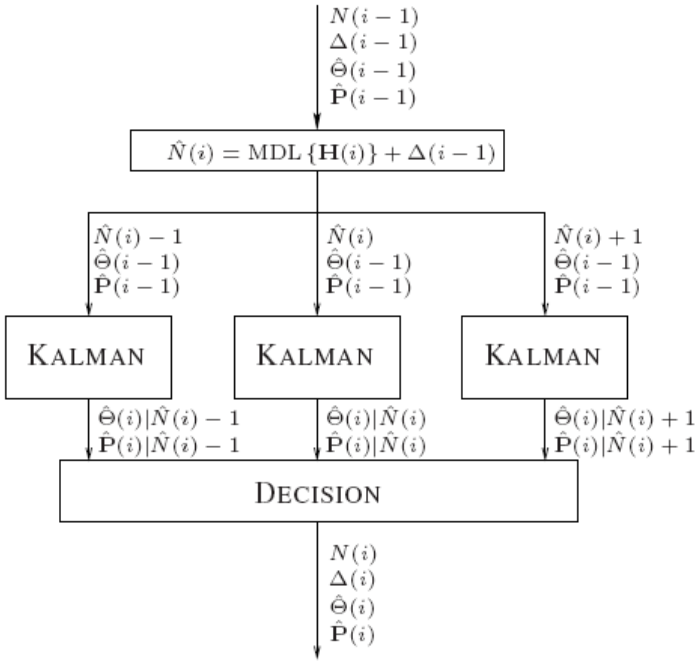

Figure 3: Flow graph of the new algorithm

and using the initialisation step in [6], where $\boldsymbol{H}\left(i \mid \hat{\Theta}(i-1), N(i-1)\right)$ is the approximation of $\boldsymbol{H}(i)$ using the model order $N(i-1)$ with the parameter vector $\hat{\Theta}(i-1)$.

- If the model order set to a tracking filter is smaller than $N(i-1)$, one or more existing paths are selected sequentially to be killed if its drop in $\hat{\Theta}(i)$ increases least the approximation quality among all paths. The approximation quality $q(\hat{\Theta}(i))$ defined as

$$q(\hat{\Theta}(i-1)) = 10\log 10\left(\frac{\left\|\boldsymbol{Res}\left(i \mid \hat{\Theta}(i-1)\right)\right\|^2}{\left[\!\left[\boldsymbol{H}(i)\right]\!\right]^2}\right) \tag{3}$$

describes the energy ratio between the residual $\boldsymbol{Res}\left(i \mid \hat{\Theta}(i-1)\right)$ and the measurement matrix $\boldsymbol{H}(i)$. In other words if $q(\hat{\Theta}(i))$ is minimal, the residual energy is small and therefore the estimated $\hat{\Theta}(i)$ matches the true values as good as possible.

$$\begin{bmatrix} \mathrm{q}\left(\hat{N}(i)-1\right) \\ \mathrm{q}\left(\hat{N}(i)\right) \\ \mathrm{q}\left(\hat{N}(i)+1\right) \end{bmatrix} = \begin{bmatrix} q(\hat{\Theta}(i)|\hat{N}(i)-1) \\ q(\hat{\Theta}(i)|\hat{N}(i)) \\ q(\hat{\Theta}(i)|\hat{N}(i)+1) \end{bmatrix} + \begin{bmatrix} -1 \\ 0 \\ 1 \end{bmatrix} \cdot p_{ord} + \begin{bmatrix} \left|N(i-1) - \left(\hat{N}(i)-1\right)\right| \\ \left|N(i-1) - \hat{N}(i)\right| \\ \left|N(i-1) - \left(\hat{N}(i)+1\right)\right| \end{bmatrix} \cdot p_{ch}\,, \tag{4}$$

After all tracking filters calculated the update step, a decision among all results is performed as shown in Figure 3 as DECISON block. Inside the decision block a model order change compared to last time step and higher model orders are penalised. This is needed as otherwise model order changes would occur too frequently with the result of paths with low power and a small life-time. The penalization of higher model orders is of the same principle as in standard model

order selection criterion [11] and is needed as the estimation problem is nested and overfitting might occur, such that paths would track noise only.

The decision process proposed here is based on the value $\boldsymbol{q}(x)$ calculated by (4) where p_{ord} as the penalty factor for higher model order and p_{ch} as the penalty value for a model order change. $q(\hat{\Theta}(i)\,|\,N(i))$ is calculated according to (3) using the estimate $\hat{\Theta}(i)$ with model order $N(i)$. The new model order at time step i, $N(i)$ is selected as

$$N(i) = \min_{x} \boldsymbol{q}(x) \tag{3}$$

with $\Delta(i) = N(i) - MDL\{\boldsymbol{H}(i)\}$.

PRELIMINARY RESULTS ON TIME-VARIANT MULTIPATH CHARACTERISTICS

The parameters of the proposed algorithm, especially the penalty factors in (4) have to be carefully chosen depending on received signal strength in order to achieve good performance. In this paper, the factors are set to 0.15 and 0.1 for p_{ord} and p_{ch} respectively. Figure 4 visualises the results for a section of 1 m on the model railway track *R2* while the transmitter was positioned above Tx-1 in height *H*2. To verify the estimation algorithm, the approximation quality $q(\hat{\Theta}(i))$ defined in last section is analysed. $q(\hat{\Theta}(i))$ is the residual to measured CIR energy ratio. A smaller value for $q(\hat{\Theta}(i))$ implies a better estimation performance, since it stands for a small residual power. For instance, a quality of -10 dB means 10% power is left as residual after estimation. However, it is worth to note that this quality is highly dependent on the received signal strength. For a low Signal-Noise-Ratio (SNR) case, the signal part in the measured CIR is small, therefore $q(\hat{\Theta}(i))$ will be higher than for a high SNR scenario.

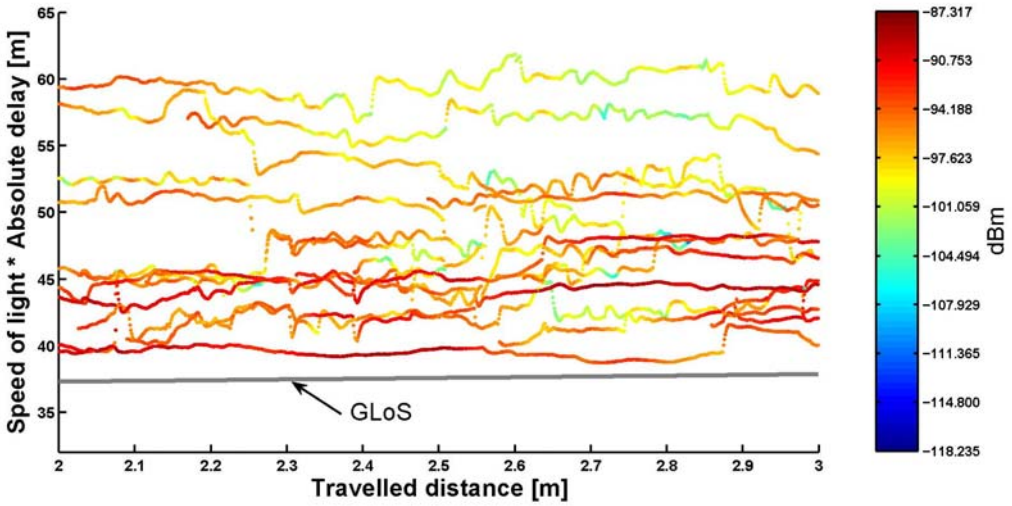

Figure 4: Example of estimated CIR within 1 m travelled distance. The light grey line shows the true GLoS distance between the transmitter and the receiver. c is the speed of light.

The left plot of Figure 5 shows the approximation quality for one track measurement where the transmitter is located above Tx-2 in a height of *H*1 while the model train was running on track *R1*. The quality is decreasing as the receiving antenna is travelling forward on *R1*. This can be explained by the received power shown in the right plot of Figure 5, which is proportional to the SNR, assuming a constant noise floor over the whole measurement. As the received signal power increases while the model train travels further, $q(\hat{\Theta}(i))$ decreases.

For time variant channels, an important parameter is the number of co-existing multipath components. As long as the receiver travels, new paths will appear and other paths will vanish. The estimated Probability Density Function (PDF) of co-existing number of paths is given by the left plot of Figure 6. A Weibull distribution shown in red is found to fit best the distribution for the number of paths. During movement of the receiving antenna, some paths are dropped due to low power and some new paths are added due to the new multipath environment. The variation in the number of paths is important which implies how often a path vanishes or appears. The right plot of Figure 6 shows the probability density function of number of paths changed between the measured neighbouring snapshots with 1 mm spatial spacing. The negative value represents the number of paths dropped and the positive value represents the number of paths added.

With a probability of 81.1%, as the receiver moves 1 mm the number of paths is not changed. A path vanishes with a probability of 9.1%, whereas a new path is detected with a probability of 9%.

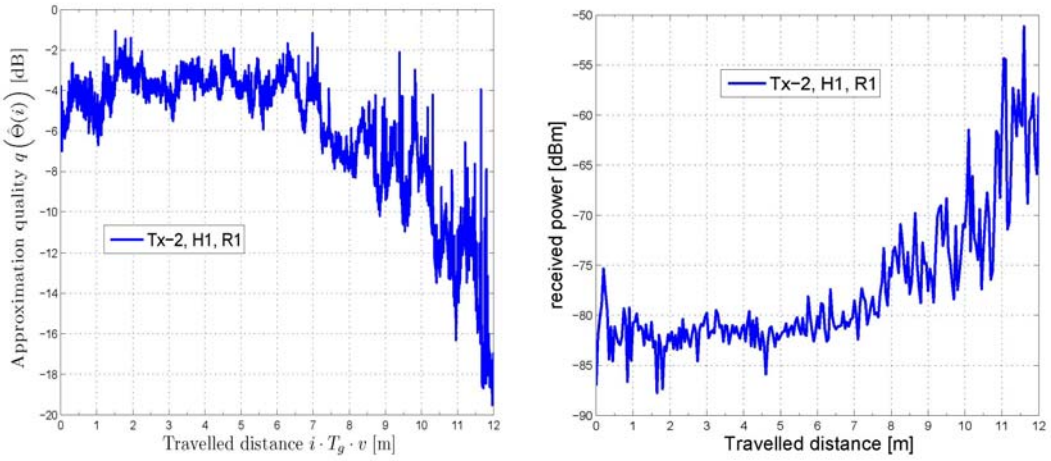

Figure 5: Left plot: approximation quality $q(\hat{\Theta}(i))$ while the receiving antenna is running on track *R1* with the transmitter located above Tx-2 in height *H*1. Right plot: the received signal power while the receiving antenna is running on track *R1* with the transmitter located above Tx-2 in height *H*1.

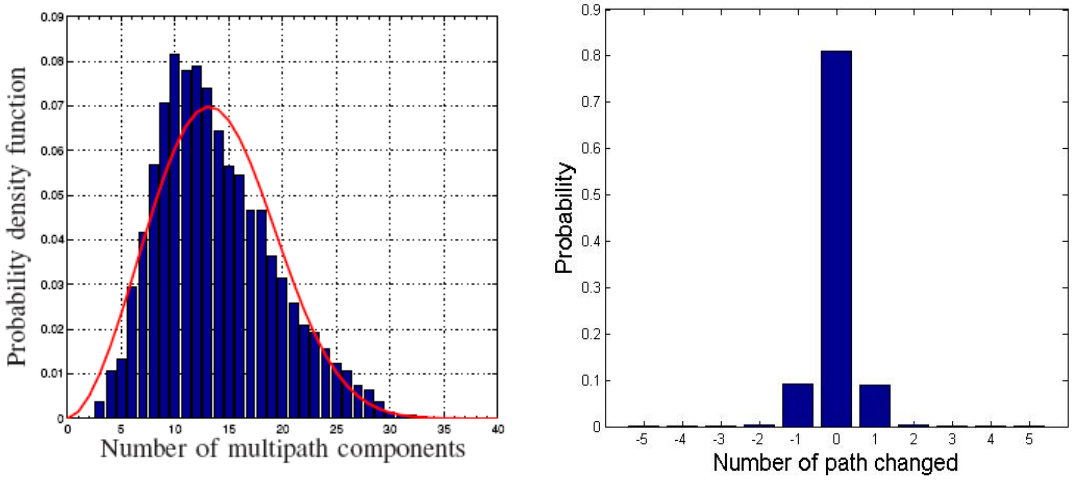

Figure 6: Left plot: histogram of the number of paths with a Weibull distribution fit as red curve. Right plot: Probability density function for a change in the number of paths between two adjacent snapshots measured in a spatial distance of 1 mm. The negative value represents a decrement of paths and positive value an increment of paths.

As described in the introduction section, the NLoS error is a key factor in the channel modelling for localization applications, which is usually not considered in communication channel models. Defined in [4] and [5], the NLoS error $\varepsilon_{NLoS}(i)$ is determined by

$$\varepsilon_{\mathrm{NLoS}}(i) = c \cdot \left(\mathrm{ToA}^{\mathrm{FP}}(i) - \mathrm{ToA}^{\mathrm{GLoS}}(i)\right) \tag{4}$$

where $\mathrm{ToA}^{\mathrm{FP}}(i)$ is the estimated delay of the first incoming path, $\mathrm{ToA}^{\mathrm{GLoS}}(i)$ is the GLoS distance between the transmitter and receiver antenna, and c denotes the speed of light. Due to estimation errors and irresolvable paths, the estimated NLoS error might be negative. For the further analysis negative values for $\varepsilon_{NLoS}(i)$ have been discarded.

The left plot of Figure 7 shows the PDF of estimated NLoS errors with an exponential distribution fit. Consistent with the findings based on the fixed point measurements on the same floor described in [5], the NLoS error can be modelled as an exponential distribution.

Due to the requirement on at least three transmitters for positioning, it is important to evaluate the link level NLoS error $\varepsilon_{NLoS}(i)$ correlation characteristics. We denote the NLoS error vector with transmitter position $d_i \in \{d1:(\text{Tx-1},H1), d2:(\text{Tx-1},H2), d3:(\text{Tx-2},H1), d4:(\text{Tx-2},H2),\}$ for a certain track $\gamma_k \in \{R1, R2\}$ as $\Im(d_i,\gamma) = [\varepsilon_{NLoS}(1), \varepsilon_{NLoS}(2), \ldots, \varepsilon_{NLoS}(Len)] \| (d_i,\gamma)$ where $(\bullet)\|(d,\gamma)$ represents the NLoS error when transmitter is located at d and receiver is running on track γ, and Len is the number of measured snapshots. The correlation coefficients $Cor(d_i,d_j,\gamma), i \neq j$, with $i, j \in \{1,2,3,4\}$, is calculated by

$$Cor(d_i,d_j,\gamma) = \frac{C_{(\Im(d_i,\gamma),\Im(d_j,\gamma))}}{\sqrt{C_{(\Im(d_i,\gamma),\Im(d_i,\gamma))} \cdot C_{(\Im(d_j,\gamma),\Im(d_j,\gamma))}}} \quad (3)$$

where $C_{(\Im(d_i,\gamma),\Im(d_j,\gamma))}$ is the cross-covariance of NLoS errors $\Im(d_i,\gamma)$ and $\Im(d_j,\gamma)$, and $C_{(\Im(d_i,\gamma),\Im(d_i,\gamma))}$ represents the auto-covariance. The corresponding correlation coefficients are listed in Table 2 for the scenarios where the transmitter is located at different horizontal positions. It can be seen that the NLoS errors of different links have no correlation in general. In other words, the NLoS errors are uncorrelated to each other. In mobile radio networks, the links to BSs from different cells would therefore result in uncorrelated NLoS errors. For channel modelling, this implies the fact that NLoS errors for different links can be generated as an independent and identically-distributed process.

To evaluate the coherence characteristics of the NLoS error, the spatial correlation of $\varepsilon_{NLoS}(i)$ for different transmitter positions and receiver tracks is investigated which is calculated as the covariance function. The result is shown in the right plot of Figure 7 where λ is the wavelength of transmitter wave. Considering a correlation level of 0.5, it can be seen that the NLoS error when receiver was running on track *R1* in corridor has longer correlated distance in spatial compared to the NLoS errors when receiver was running on track *R2* in wide area room. For former case, the correlated distance is up to 40 λ, whereas for the latter case the correlated distance is up to 4 λ.

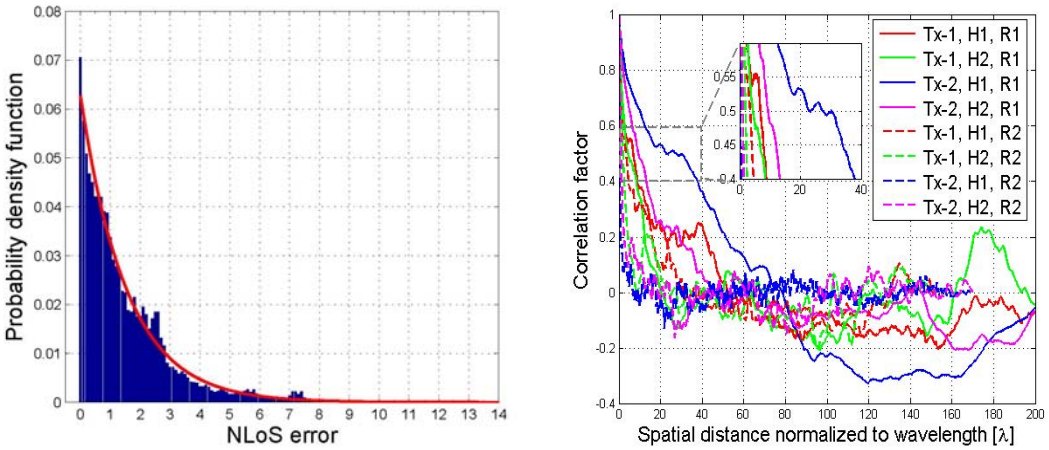

Figure 7: Left plot: Histogram of the NLoS error with an exponential fit as red curve. Right plot: the spatial correlation characteristics of NLoS error for different transmitter positions and receiver tracks.

Table 2: Inter-Link Correlation coefficients of NLoS Error

	γ	
	R1	*R2*
$Cor(d_1,d_3,\gamma)$	-0.4335	0.0056
$Cor(d_1,d_4,\gamma)$	-0.2195	0.0762
$Cor(d_2,d_3,\gamma)$	0.1661	0.1233
$Cor(d_2,d_4,\gamma)$	0.1896	0.0510

CONCLUSIONS

In order to model the time variant multipath components for location/navigation applications, we proposed a new SAGE based Kalman filter to effectively estimate and track the parameters of time variant paths. Based on an outdoor to indoor broadband wireless channel measurement campaign, the time-variant channel characteristics are estimated and modelled. As one important parameter for positioning applications, the NLoS error is demonstrated to be exponential distributed, and inter-link NLoS errors can be generated as an independent and identically-distributed process. It has also been shown that the spatial correlation distance of NLoS error in corridor is generally longer than that in wide area room. The number of multipaths is modelled by a Weibull distribution. For most of the time, the number of co-existing paths does not change when the receiving antenna is moved by 1mm. With a probability of 18.1% the number of paths is changed by 1.

REFERENCES

[1] C. Mensing, S. Sand, A. Dammann, and W. Utschick, "Interference-Aware Location Estimation in Cellular OFDM Communications Systems," *IEEE International Conference on Communications (ICC)*, Dresden, Germany, June 2009.

[2] —, "Location Estimation in Cellular OFDM Communications Systems," *IEEE Global Communications Conference (GLOBECOM)*, Honolulu, USA, November/December 2009.

[3] D. Baum, J. Hansen, J. Salo, G. Galdo, M. Milojevic, and P. Kyosti, "An Interim Channel Model for Beyond-3G Systems Extending the 3GPP Spatial Channel Model (SCM)," *IEEE Vehicular Technology Conference (VTC Spring)*, Stockholm, Sweden, May/June 2005.

[4] W. Wang, T. Jost, and A. Dammann, "Outdoor to Indoor Channel Characteristics on Two Difference Floors," *European Transaction on Telecommunications (ETT)*, vol.5, to appear, 2010.

[5] W. Wang and T. Jost, "Multiple-Links NLoS Error Evaluation for Geolocation Channel Modelling," *IEEE Vehicular Technology Conference (VTC Spring)*, Taipei, Taiwan, May 2010.

[6] B. Fleury, M. Tschudin, R. Heddergott, D. Dahlhaus, and K. Pedersen, "Channel Parameters Estimation in Mobile Radio Environments Using the SAGE Algorithm," *IEEE Journal on Selected Areas in Communications*, vol. 17, no. 3, pp. 434-450, March, 1999.

[7] A. Richter, "Estimation of Radio Channel Parameters: Models and Algorithm," Ph.D Dissertation, 2005, ISBN: 978-3-938843-02-4.

[8] A. Lehner, "Multipath Channel Modelling for Satellite Navigation Systems," Ph.D Dissertation, 2007, ISBN: 978-3-8322-6651-6.

[9] J. Salmi, A. Richter, and V. Koivunen,, "Detection and Tracking of MIMO Propagation Path Parameters Using State-Space Approach," *IEEE Transaction on Signal Processing*, vol. 57, no. 4, pp. 1538-1550, April, 2009.

[10] T. Jost and W. Wang, "Satellite-to-Indoor Broadband Channel Measurements at 1.51GHz," *ION International Technical Meeting (ITM)*, Anaheim, USA, January, 2009.

[11] P. Stoica and Y. Selen, "Model-order selection: a review of information criterion rules," *IEEE Signal Processing Magazine*, vol. 21, no. 4, pp. 36-47, July, 2004.

A.2 Estimation and Modelling of NLoS Time-Variant Multipath for Localization Channel Model in Mobile Radios

W. Wang, T. Jost, and A. Dammann. Estimation and modelling of nlos time-variant multipath for localization channel model in mobile radios. In *The IEEE Global Communications Conference (GLOBECOM 2010)*, Miami, USA, December 2010.

Estimation and Modelling of NLoS Time-Variant Multipath for Localization Channel Model in Mobile Radios

Wei Wang, Thomas Jost, and Armin Dammann

German Aerospace Center (DLR)
Institute of Communications and Navigation
Oberpfaffenhofen, 82234 Wessling, Germany
Email: {Wei.Wang, Thomas.Jost, Armin.Dammann}@DLR.de

***Abstract*—Time Based (TB) localization in terrestrial communications mobile radio as a complementation to global navigation satellite systems has gained recently plenty of interests. As an essential tool to develop suitable algorithms for joint communications and localizations in mobile radio networks, the wireless channel model has a growing significance. For both communications and localizations, the time evolution of multipath components is essential especially for tracking applications. Moreover, the Non Line-of-Sight (NLoS) error due to an undetectable line-of-sight path introduces an additional range error for TB localizations, which needs to be taken into account in the channel model. In this paper we present a space-alternating generalized expectation-maximization based Kalman filter method to efficiently estimate and track the time-variant multipath components based on a channel measurement campaign. The modeling of time-variant multipath characteristics, in terms of NLoS error, variance of path number, and the life span, are presented in this paper as well.**

I. Introduction

Positioning by using Global Navigation Satellite Systems (GNSSs), such as the Global Positioning System (GPS) operating at L-band, promises very accurate location information, when a Line-of-Sight (LoS) condition to the satellite is present. However, positioning in urban canyons, where LoS might be absent, GNSSs do not provide accurate positions. For some indoor areas, like rooms with metallized windows, satellite signals can not be tracked by GPS receivers because of low signal power. Time Based (TB) localization, utilizing available ground communication networks [1] [2], are investigated as a complementation to GNSS with the advantage of higher signal power level in comparison. By suitable Hybrid Data Fusion (HDF) algorithms to combine measures obtained from GNSS and terrestrial networks, the accuracy of the estimated position can be improved.

As an essential tool for receiver development in terms of TB localization in communication networks, wireless channel modelling has a growing significance. Due to a dissimilar focus between communications and positioning, channel models for both applications are different.

- For communications in mobile radio networks, multipath modelling is more used to evaluate the Bit Error Rate (BER) [3], and is considered as the most essential criterion for algorithms evaluation, like channel estimation, coding/decoding, and synchronization.
- TB positioning using mobile radio networks focuses on investigating of the position error, which is directly related to the range error of individual links. Two different major channel characteristics effect the range error. Firstly, the ranging based on the first detectable wave is positively biased if the Geometrical Line-of-Sight (GLoS) path is blocked. Generally this bias, between the geometrical distance from the transmitter to the receiver and the propagation distance of the first detectable path is known as the Non Line-of-Sight (NLoS) error [4] [5]. Secondly due to multipath the correlator based synchronizer which is generally used for range estimation is biased positively or negatively by the superposition of paths [2].

In realistic scenarios for location-tracking/navigation applications, the multipaths are time-variant in delays, amplitudes, phases and incoming angles due to movements of transmitters, receivers, and/or reflectors. Therefore, it is essential to model the time evolution for each path, e.g., its life-time. Estimation of time-variant multipath parameters from channel measurement data is usually based on an underlying snapshot based estimator like the Space-Alternating Generalized Expectation-maximization (SAGE) algorithm [6] or RIMAX [7] and an attached path detection scheme as in [8]. Snapshot based algorithms do not consider the previous or consequent time information and are therefore non-optimal. With the fact that the multipath parameters vary slowly in time, some alternative algorithms have been proposed by utilizing a variable state dimension Extended Kalman Filter (EKF) to track propagation paths parameters [9]. However, applying the EKF inherently means using a first order polynomial approximation, which is inadequate in scenarios where closed space multipath is present. In such a situation the filter might loose its lock on tracking the global a-posteriori maximum and track local maxima or disconverges completely. Besides, [10] applied a particle filter algorithm to overcome the problem of the non-linear measurement model with the drawback of an increased computational complexity. For practical application of the algorithm, one particle filter per path is proposed, which limits the usability of the algorithm to scenarios, where paths are very distinct and independent in their features and influences on the measurement data.

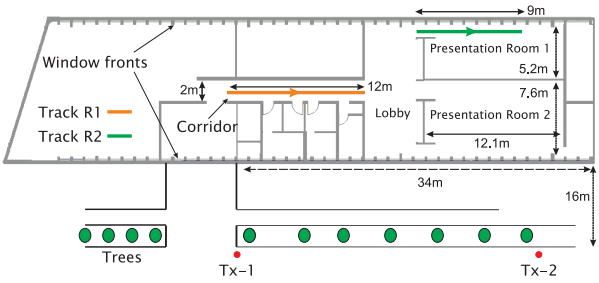

Fig. 1. Building layout with track $R1$ and $R2$. Tx-1 and Tx-2 indicate azimuth positions of the transmitter. All rooms are located on the high-level of the building, which is ≈ 9 m above the ground.

In this paper, we utilize a SAGE based Kalman Filter (KF) method to estimate and track the multipath based on a dynamic Single Input Single Output (SISO) measurement. 1-D Angle of Arrival (AoA) information is used by utilizing a Virtual Antenna Array (VAA) in post-processing.

In Section II, the setup of the channel measurement campaign is briefly addressed. Thereafter, the SAGE based KF method is presented in Section III. In Section IV the estimated results of the proposed methods and the modeling of multipath components are presented. Finally Section V concludes this paper.

II. Channel Measurement Campaign

A. Measurement Setup and Environments

The measurement was accomplished in the SISO manner with a MEDAV RUSK broadband channel sounder at premises of the German Aerospace Center (DLR). A spread signal — in particular an Orthogonal Frequency Division Multiplexing (OFDM) signal — has been sent by the transmitter. The parameter setup of the channel sounder is summarized in Table I. The measured i-th snapshot of the Channel Impulse Response

TABLE I
Channel sounder settings for the measurement

RF centre frequency	5.2 GHz
Bandwidth	$B = 120$ MHz with 1537 sub-carrier
Transmit Power	5 W $\cong$ 37 dBm
Signal period	12.8 μs
Measurement time grid	1.024 ms
Antennas	Omni-directional (V-polarised)

(CIR), $h(i,j)$, $j = 0,\ldots,M-1$ consists of $M = 1537$ samples at delays $\tau_j = j\Delta\tau$, with $\Delta\tau = 1/B$. The channel sounder records one CIR every $T_g = 1.024$ ms providing a measurement rate of 976 CIRs per second (CIRs/s).

The measurement was performed on the second floor (9 m above ground) of the building characterized as a standard three story office building of concrete with non-metallic window glass as described in [11]. In order to perform the dynamic measurement, the receiving antenna was mounted on a model train running along two tracks $R1$ and $R2$ planted on the ground with a speed of $v \approx 0.15$ m/s, where no LoS is present as displayed in Fig. 1. The transmitter was positioned above the points Tx-1 and Tx-2 as shown in Fig. 1 in heights of $H1 = 12$ m and $H2 = 18$ m. So overall four

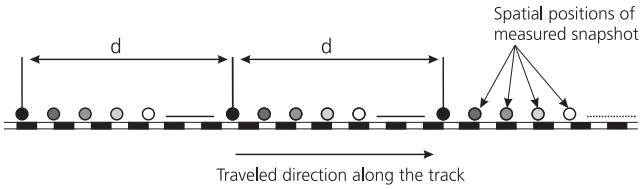

Fig. 2. VAA generation from the measurement

different transmitter positions were achieved. The position of the transmitter was precisely determined using a Leica tachymeter giving a nominal accuracy in the sub-cm domain. To get a similar accuracy for the receiver antenna mounted on the model train, the train is equipped with a rotary encoder giving 500 impulses per motor turn as described in [11]. To prevent wheel slipping the model train runs with a cogwheel. Together with each CIR snapshot measurement $h(i,j)$ the number of impulses given by the rotary encoder, since the model train started to move, is saved, which results in a precise travelled distance measure for each captured impulse response snapshot. To validate the accuracy of the distance measurement by rotary encoder, $k = 1,\ldots,K$, with $K = 21$ train runs have been performed. The K distance errors between estimated travelled distances $\hat{d}_k$ and the real distances d_k have a mean value of 0.16 mm/m and a standard deviation of 0.14 mm/m. As the time of arrival is the most important value for navigation receivers and therefore the most important part in this measurement campaign, receiver and transmitter were perfectly synchronized by cable connection using one common rubidium atomic clock serving as frequency normal. This setup prevents time drifts which usually occur in channel sounder measurements using separated clocks.

B. VAA Processing

Generally, estimation of AoA information with an antenna array takes the benefit of incoming phase differences of different antenna elements. As described in Section II-A, the measurement was performed in the SISO manner with a single antenna which does not provide spatial phase difference information. However, it is possible to extract a linear antenna array from the measurement due to the utilization of rotary encoder. The distance error per meter estimated through the odometer measurement is 0.16 mm/m in average, which is small enough to be ignored. As a result, it is possible to form a uniform linear VAA with element-spacing d as shown in Fig. 2. In this paper, the train movement direction is defined as the travelling direction, meaning that for the receiver antenna positioned at the end of the track a ray coming from the start point of the track has a AoA of 0°. The receiver was running from the left to the right for tracks $R1$ and $R2$ as depicted in Fig. 1. A VAA snapshot is defined as $\mathbf{h}(i) = [\underline{h}(i),\ldots,\underline{h}(i+(N_E-1)\cdot d)]^T$, where $(\cdot)^T$ stands for vector or matrix transpose, N_E is the number of elements, and $\underline{h}(i) = [h(i,0),\ldots,h(i,M-1)]^T$. The Fourier transform, denoted as $\mathcal{F}\{\cdot\}$, of $\mathbf{h}(i)$ shall be further defined as $\mathbf{H}(i) = \mathcal{F}\{\mathbf{h}(i)\}$, where each row of $\mathbf{h}(i)$ is separately Fourier transformed. More details on the VAA and SAGE processing can be found in [4].

III. SAGE Based KF Method for Multipath Estimation and Tracking

The purpose of the method described here, is to track the parameter vector $\theta_l(i) = [a_l(i), \vartheta_l(i), \tau_l(i), \Delta a_l(i), \Delta\vartheta_l(i), \Delta\tau_l(i)]^T$, for each path l, with $l = 1, \ldots, N(i)$. The elements of $\theta_l(i)$ are the complex amplitude $a_l(i)$, its AoA $\vartheta_l(i)$, its delay $\tau_l(i)$ as well as the rates $\Delta a_l(i)$, $\Delta\vartheta_l(i)$ and $\Delta\tau_l(i)$. The state vector $\Theta(i)$ of the KF describes the states for all paths as $\Theta(i) = \left[\theta_1(i)^T, \ldots, \theta_{N(i)}(i)^T\right]^T$.

Instead of taking directly $\hat{\mathbf{H}}(i)$ as measurement into the tracking filter as done in [9], a maximum search converging to the next maximum of the likelihood function around the prediction $\hat{\Theta}^-(i)$ is used. This yields a faster convergence of the tracking filter over time i as well as a more robust behavior.

For the maximum likelihood search, the SAGE algorithm [6] is favored denoted by $S\{\mathbf{H}(i), \hat{\Theta}^-(i)\}$. The initialization of the SAGE is given by the predicted value $\hat{\Theta}^-(i)$ from the KF. The Kalman filter as the outer estimator is defined by

$$\begin{aligned}
\hat{\Theta}^-(i) &= \mathbf{F} \cdot \hat{\Theta}(i-1) \\
\hat{\mathbf{P}}^-(i) &= \mathbf{F} \cdot \hat{\mathbf{P}}(i-1) \cdot \mathbf{F}^H + \mathbf{W} \\
\mathbf{K} &= \hat{\mathbf{P}}^-(i) \cdot \mathcal{H}_n^H \cdot \left[\mathcal{H}_n \cdot \hat{\mathbf{P}}^-(i) \cdot \mathcal{H}_n^H + \mathbf{R}\right]^{-1} \\
\hat{\Theta}(i) &= \hat{\Theta}^-(i) + \mathbf{K} \cdot \left[S\{\mathbf{H}(i), \hat{\Theta}^-(i)\} - \mathcal{H}_n \cdot \hat{\Theta}^-(i)\right] \\
\hat{\mathbf{P}}(i) &= \left(\mathbf{I} - \mathbf{K} \cdot \mathcal{H}_n\right) \hat{\mathbf{P}}^-(i)\,,
\end{aligned}$$

where $\mathcal{H}_n$ represents a simple mapping matrix between the state vector $\hat{\Theta}^-(i)$ and the values calculated in the SAGE algorithm. $\mathbf{F}$ represents the state transition matrix in the system equation, $\mathbf{W}$ the covariance of the process noise, and $\mathbf{K}$ the Kalman gain matrix. The covariance of the measurement noise $\mathbf{R}$ is the inverse of the Fisher information matrix, which is simplified as diagonal matrix.

Fig. 3 displays the overall routine including the model order selection part. The initialization for $i = 1, 2$ is simply performed by SAGE, so that the $\Delta(0)$ is obtained. From the last time step $i-1$ the model order $N(i-1)$, $\Delta(i-1)$ and the tracking results $\hat{\Theta}(i-1)$ and $\hat{\mathbf{P}}(i-1)$ are used. $\Delta(i)$ represents an additive factor to the model order selection criteria based on each snapshot as shown in Fig. 3. For model order selection the Minimum Description Length (MDL) [12], using the sample covariance matrix for decreasing the computational complexity, is utilised.

After calculating the new model order at time i, $\hat{N}(i)$, several tracking filters (denoted in Fig. 3 only as KALMAN) are running in parallel each with a different model order around the estimated $\hat{N}(i)$.

- If the model order set to a tracking filter is larger than $N(i-1)$, new paths are initialised by calculating the residual sequence

$$\mathbf{Res}(i|\hat{\Theta}(i-1)) = \mathbf{H}(i) - \mathbf{H}(i|\hat{\Theta}(i-1), N(i-1)) \quad (1)$$

  and using the initialisation step in [6], where $\mathbf{H}(i|\hat{\Theta}(i-1), N(i-1))$ is the approximation of $\mathbf{H}(i)$ using the model order $N(i-1)$ with the parameter vector $\hat{\Theta}(i-1)$.

- If the model order set to a tracking filter is smaller than $N(i-1)$, one or more existing paths are selected sequentially to be killed if its drop in $\hat{\Theta}(i)$ increases least the approximation quality among all paths. The approximation quality $q(\hat{\Theta}(i))$ defined as

$$q(\hat{\Theta}(i)) = 10\,\log_{10}\left(\frac{\|\mathbf{Res}(i|\hat{\Theta}(i-1))\|^2}{\|\mathbf{H}(i)\|^2}\right), \quad (2)$$

  describes the energy ratio between the residual $\mathbf{Res}(i|\hat{\Theta}(i-1))$ and the measurement matrix $\mathbf{H}(i)$. In other words if $q(\hat{\Theta}(i))$ is minimal, the residual energy is small and therefore the estimated $\hat{\Theta}(i)$ matches the true values as good as possible.

After all tracking filters calculated the update step, a decision among all results is performed as shown in Fig. 3 as DECISION block. Inside the decision block a model order change compared to last time step and higher model orders are penalised. This is needed as otherwise model order changes would occur too frequently with the result of paths with low power and a small life-time. The penalization of higher model orders is of the same principle as in standard model order selection criterion [12] and is needed as the estimation problem is nested and overfitting might occur, such that paths would track noise only. p_{ord} can be straightforwardly calculated according to the information criterion rules, e.g., MDL.

The decision process proposed here is based on the value $\mathbf{q}(x)$ calculated by Eq. (3) where p_{ord} as the penalty factor for higher model order and p_{ch} as the penalty value for a model order change. $q(\hat{\Theta}(i)|N(i))$ is calculated according to Eq. (2) using the estimate $\hat{\Theta}(i)$ with model order $N(i)$. The new model order at time step i, $N(i)$ is selected as

$$N(i) = \min_x \mathbf{q}(x)$$

with $\Delta(i) = N(i) - \mathrm{MDL}\{\mathbf{H}(i)\}$.

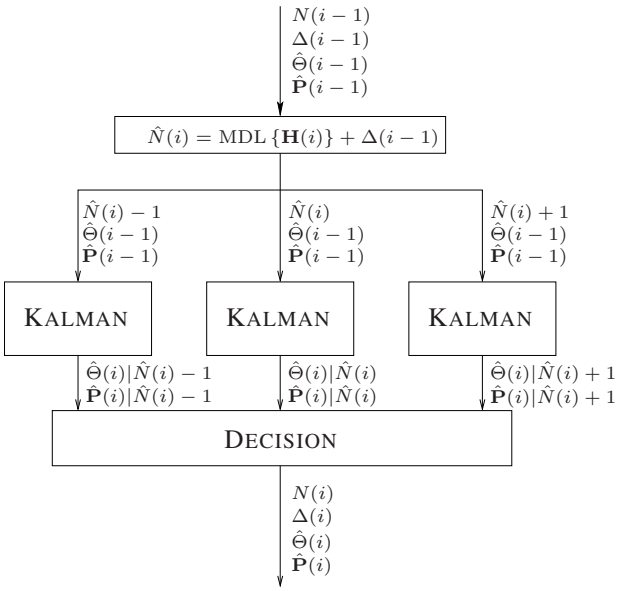

Fig. 3. Flow graph of the new algorithm

$$\begin{bmatrix} \mathbf{q}\left(\hat{N}(i)-1\right) \\ \mathbf{q}\left(\hat{N}(i)\right) \\ \mathbf{q}\left(\hat{N}(i)+1\right) \end{bmatrix} = \begin{bmatrix} q(\hat{\Theta}(i)|\hat{N}(i)-1) \\ q(\hat{\Theta}(i)|\hat{N}(i)) \\ q(\hat{\Theta}(i)|\hat{N}(i)+1) \end{bmatrix} + \begin{bmatrix} -1 \\ 0 \\ 1 \end{bmatrix} \cdot p_{ord} + \begin{bmatrix} \left|N(i-1)-\left(\hat{N}(i)-1\right)\right| \\ \left|N(i-1)-\hat{N}(i)\right| \\ \left|N(i-1)-\left(\hat{N}(i)+1\right)\right| \end{bmatrix} \cdot p_{ch}\,, \tag{3}$$

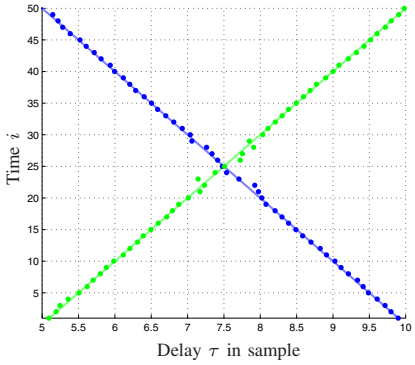

Fig. 4. Simulation scenario-1, where each line represents a path along time. The points are estimates using the proposed method while the line indicates the true values. The color represents a path respectively points belonging togethers.

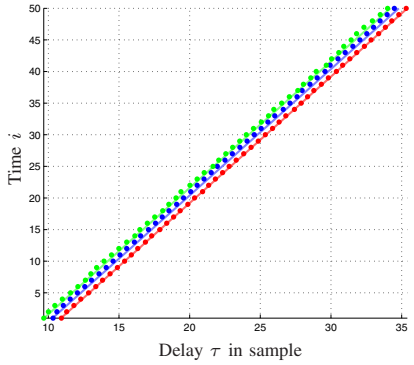

Fig. 5. Simulation scenario-2, where each line represents a path along time. The points are estimates using the proposed method while the line indicates the true values. The color represents a path respectively points belonging togethers.

IV. Time-Variant Multipath Characteristics

A. Analytical Simulations within Controlled Environments

To verify the robustness in tracking, two analytical simulations are performed. The first simulation scenario consists of two paths crossing each other as shown in Fig. 4, while the second scenario surveys a situation where three paths are running in parallel as shown in Fig. 5. The colored solid lines represent the true path along time with constant complex amplitude of 1 for all paths. The CIR length in the simulation is fixed to 101 samples, and the signal-to-noise ratio is 20 dB. The transition matrix $\mathbf{F}$ is taken as an identity matrix as well as for $\mathbf{W}$ and $\mathbf{R}$. For all simulations the model order determination is assumed as perfect. The evaluation of the performance is based on the sum of squared errors $m(i)$ defined as

$$m(i) = \sum_{l=0}^{N(i)-1} |\hat{\tau}_l(i) - \tau_l(i)|^2 + |\hat{\alpha}_l(i) - \alpha_l(i)|^2 \tag{4}$$

where $\hat{\tau}_l(i)$ and $\hat{\alpha}_l(i)$ denotes the estimates of $\tau_l(i)$ and $\alpha_l(i)$ at time i respectively.

The simulation results for scenario-1 are shown in Fig. 6 comparing the EKF in [9] with the proposed algorithm. Both algorithms are tracking two paths sufficiently up to $i \approx 20$, when both paths are still well separated from each other in delay. As the two paths are getting closer in delay, they interfere with each other which increases the estimation error as visible in Fig. 6 around $i = 25$. After the two paths did cross, the EKF disconverges, so looses its lock in the tracking in 12 out of 100 simulated cases while the proposed algorithm disconverges in only 5% of the simulated runs. The situation gets even more severe for scenario-2 depicted in Fig. 7. Among

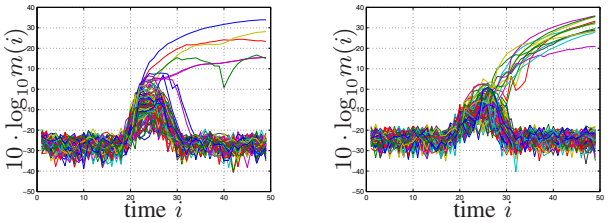

(a) Proposed method. (b) EKF in [9].

Fig. 6. Error results for scenario-1 with the proposed method and the EKF in [9]. Displayed are the results of 100 simulation runs.

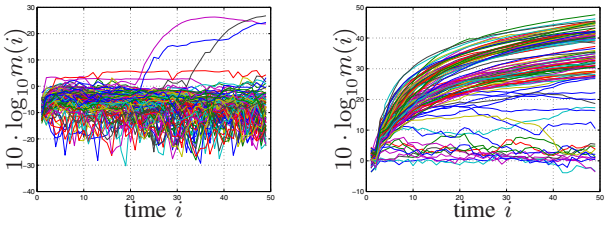

(a) Proposed method. (b) EKF in [9].

Fig. 7. Error results for scenario-2 with the proposed method and the EKF in [9]. Displayed are the results of 100 simulation runs.

the results obtained from 100 simulations, the tracking by EKF looses in nearly every case while the proposed algorithm shows a very robust behavior with only 3% failure rate.

B. Estimation of Multipath Parameters Based on Measurements

The parameters of the proposed algorithm, especially the penalty factors in Eq. (3) have to be carefully chosen depending on received signal strength in order to achieve good

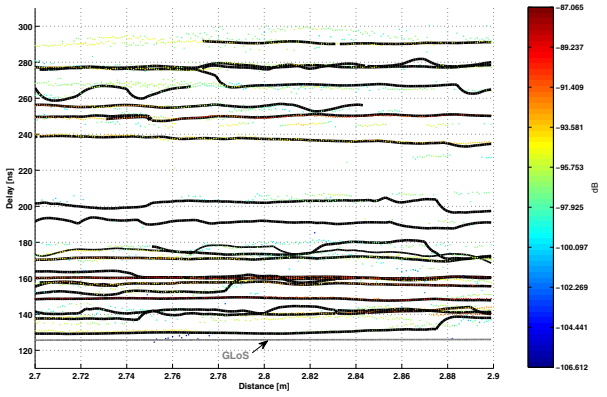

Fig. 8. Example of estimated CIR within 0.2 m travelled distance. The light grey line shows the true GLoS distance between the transmitter and the receiver. Color dots are estimated with pure SAGE, and black lines are the estimates with proposed method. c is the speed of light.

performance. In this paper, the factors are set to 0.15 and 0.1 for p_{ord} and p_{ch} respectively. Fig. 8 visualises the results for a section of 0.2 m on the model railway track $R2$ while the transmitter was positioned above Tx-1 in height $H2$. The color dots are estimates using the snapshot-based SAGE algorithm, whereas the black lines are estimates using the proposed algorithm.

1) NLoS Error Characteristics: As described in Section I, the NLoS error is a key factor in the channel modelling for localization applications, which is usually not considered in communication channel models. Defined in [4] and [5], the NLoS error $\varepsilon_{\mathrm{NLoS}}(i)$ is determined by

$$\varepsilon_{\mathrm{NLoS}}(i) = c \cdot \left(\mathrm{ToA}^{\mathrm{FP}}(i) - \mathrm{ToA}^{\mathrm{GLoS}}(i)\right) \tag{5}$$

where $\mathrm{ToA}^{\mathrm{FP}}(i)$ is the estimated delay of the first incoming path, $\mathrm{ToA}^{\mathrm{GLoS}}(i)$ is the true GLoS distance between the transmitter and receiver antenna, and c denotes the speed of light. Due to estimation errors and irresolvable paths, the estimated NLoS error might be negative. For the further analysis negative values for $\varepsilon_{\mathrm{NLoS}}(i)$ have been discarded.

Fig. 9 shows the Probability Density Function (PDF) of estimated NLoS errors with an exponential distribution fit based on maximum likelihood estimation. Consistent with the findings based on the fixed point measurements on the same floor described in [5], the NLoS error can be modelled as an exponential distribution.

2) Co-Existing Multipath Components: For time variant channels, an important parameter is the number of co-existing multipath components. As long as the receiver travels, new paths will appear and other paths will vanish. The statistical PDF of the amount of co-existing paths is given in Fig. 10. A Weibull distribution shown as red curve is found to fit best the distribution of number of multipath based on maximum likelihood estimation. During movement of the receiving antenna, the variation in the number of paths is important which implies how often a path vanishes or appears. Fig. 11 depicts the spatial correlation characteristics of the path number for each track measurement. Considering the correlation level of 0.5,

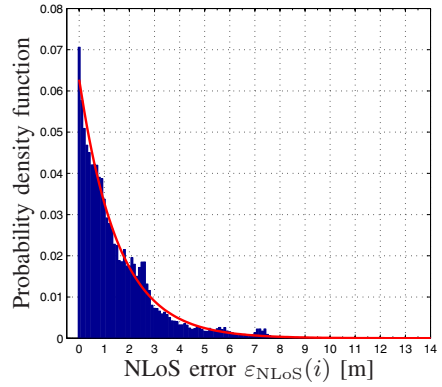

Fig. 9. Histogram of NLoS error $\varepsilon_{\mathrm{NLoS}}(i)$ with an exponential fit in red curve

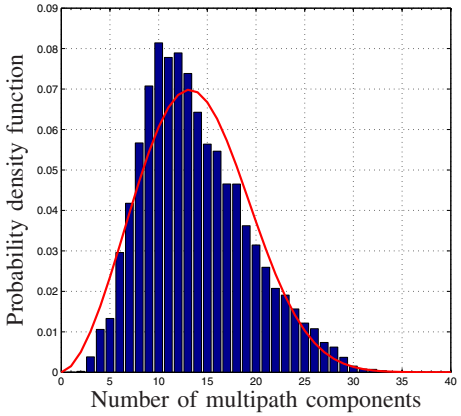

Fig. 10. Histogram of co-existing multipath numbers with a Weibull distribution fit in red curve

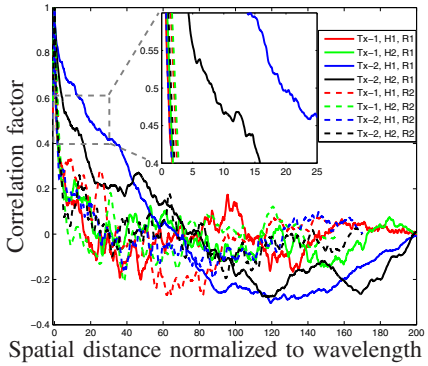

Fig. 11. Spatial correlation properties of the number of co-existing multipath

most track measurements show a correlation distance of 2λ, where λ denotes the wavelength. For scenarios with relatively high received power, where transmitter located above Tx-2 and model train ran on $R1$, the number of paths varies much slower.

3) Multipath Life Span: Due to the movement of transmitter, receiver or reflector, multipath parameters change over

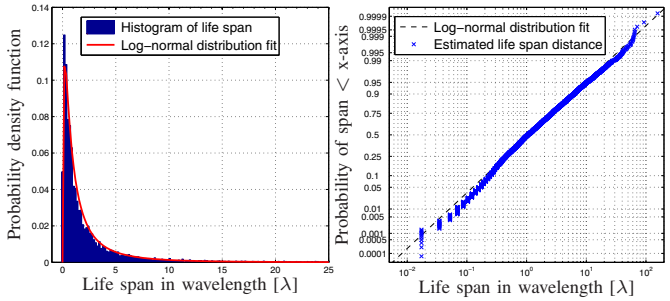

Fig. 12. Left plot: histogram of life span in wavelength with a Log-normal distribution fit in red curve; right plot: probability plot for life span with Log-normal distribution fit

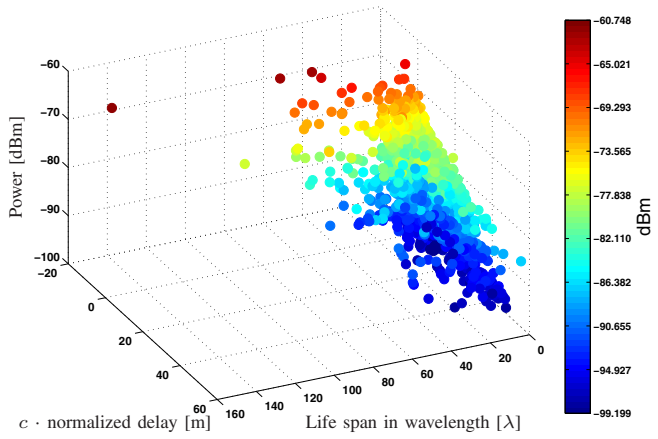

Fig. 13. Multipath components scatter plot of mean normalized delay multiplied by speed of light, mean power, and life span. Each color-coded dot represent one multipah component.

time in delay, amplitude, and AoA in general. As long as the receiving antenna is in movement, new paths appear and other paths vanish in the performed measurement. The estimated life span in terms of receiver travelled distance for multipath components of all track measurements is shown in Fig. 12. The Log-normal distribution seems to model the life span well as shown on the right side of Fig. 12. Generally paths have a life span of approximately 5λ. The maximum life span measured is 158λ. Each multipath component is characterized by a life span, a time variant AoA, amplitude and delay. To analyse the properties for each multipath component, the mean values of the AoA, the power and the delay are taken. The delays are normalized to the GLoS delay, such that a LoS signal would have a delay of value zero. Fig. 13 shows the scatter plot of the mean normalized delay multiplied by the speed of light, mean power, and life span. Each color-coded dot represents a multipath component. Only the multipaths with higher received power have long life spans. They are usually close to the GLoS delay. For multipath components with a low average received power the life span is usually short.

V. Conclusions

In order to model the time variant multipath components for location/navigation applications, we proposed a new SAGE based Kalman filter to effectively estimate and track the parameters of time variant paths. Based on an outdoor to indoor broadband wireless channel measurement campaign, the channel characteristics are estimated and modelled. As one important parameter for positioning applications, the NLoS error is demonstrated to be exponential distributed. The number of multipaths could be modelled by a Weibull distribution and their spatial correlation indicates the variation of the number of paths. As another characteristic of multipath components, the path life span estimated from the measurement is up to 158λ, but mostly less than 10λ. A Log-normal distribution is proposed as life span modeling.

Acknowledgment

This work was founded by the DLR internal project Galileo ADvanced APplications (GalileoADAP). The authors would like to thank Christian Mensing, Kai Wendlandt, Frank Schubert, Michael Walter, and Uwe-Carsten Fiebig for their support during the measurement.

References

[1] C. Mensing, S. Sand, A. Dammann, and W.Utschick, "Interference-Aware Location Estimation in Cellular OFDM Communications Systems," in *IEEE International Conference on Communications (ICC)*, Dresden, Germany, June 2009.

[2] ——, "Location Estimation in Cellular OFDM Communications Systems," in *IEEE Global Communications Conference (GLOBECOM)*, Honolulu, USA, November/December 2009.

[3] D. Baum, J. Hansen, J. Salo, G. Galdo, M. Milojevic, and P. Kyosti, "An Interim Channel Model for Beyond-3G Systems Extending the 3GPP Spatial Channel Model (SCM)," in *IEEE Vehicular Technology Conference (VTC Spring)*, Stockholm, Sweden, May/June 2005.

[4] W. Wang, T. Jost, and A. Dammann, "Outdoor to Indoor Channel Characteristics on Different Floors," *European Transactions on Telecommunications (ETT)*, vol. 21, no. 5, August 2010.

[5] W. Wang and T. Jost, "Multiple-Links NLoS Error Evaluations for Geolocation Channel Modelling," in *IEEE Vehicular Technology Conference (VTC Spring)*, Taipei, Taiwan, May 2010.

[6] B. Fleury, M. Tschudin, R. Heddergott, D. Dahlhaus, , and K. Pedersen, "Channel Parameter Estimation in Mobile Radio Environments Using the SAGE Algorithm," *IEEE Journal on Selected Areas in Communications*, vol. 17, no. 3, pp. 434–450, March 1999.

[7] A. Richter, "Estimation of Radio Channel Parameters: Models and Algorithms," Ph. D. dissertation, 2005, ISBN: 978-3-938843-02-4.

[8] A. Lehner, "Multipath Channel Modelling for Satellite Navigation Systems," Ph. D. dissertation, 2007, ISBN: 978-3-8322-6651-6.

[9] J. Salmi, A. Richter, and V. Koivunen, "Detection and tracking of MIMO propagation path parameters using state-space approach," *IEEE Transactions on Signal Processing*, vol. 57, no. 4, pp. 1538–1550, Apr. 2009.

[10] X. Yin, G. Steinboeck, G. Kirkelund, T. Pedersen, P. Blattnig, A. Jaquier, and B. Fleury, "Tracking of Time-Variant Radio Propagation Paths using Particle Filtering," in *IEEE International Conference on Communications (ICC)*, Beijing, China, May 2008.

[11] T. Jost and W. Wang, "Satellite-to-Indoor Broadband Channel Measurements at 1.51 GHz," in *ION International Technical Meeting (ITM)*, Anaheim, USA, January 2009.

[12] P. Stoica and Y. Selen, "Model-order selection: a review of information criterion rules," *IEEE Signal Processing Magazine*, vol. 21, no. 4, pp. 36–47, Jul. 2004.

A.3 Outdoor to Indoor Channel Characteristics on two Different Floors

W. Wang, T. Jost, and A. Dammann. Outdoor to Indoor Channel Characteristics on Different Floors. *European Transactions on Telecommunications (ETT)*, 21(5), Aug. 2010.

EUROPEAN TRANSACTIONS ON TELECOMMUNICATIONS
Eur. Trans. Telecomms. 2010; **21**:426–434
Published online 8 June 2010 in Wiley InterScience
(www.interscience.wiley.com) DOI: 10.1002/ett.1424

Outdoor to indoor channel characteristics on two different floors†

Wei Wang*, Thomas Jost and Armin Dammann

Institute of Communications and Navigation, German Aerospace Center (DLR), Oberpfaffenhofen, 82234 Wessling, Germany

SUMMARY

Recently the fusion of positioning and wireless communication has gained many interests due to the merits of location information for future communication systems. Both positioning and wireless communication are highly dependent on the air channel. Current channel models are well suited for communication applications but less for positioning. Therefore, we investigate and compare the channel characteristics of different floors in favour of positioning based on an outdoor to indoor broadband channel sounder measurement campaign. Power delay profiles on both floors show similar structure caused by outdoor wave propagation, and angle of arrivals mostly arrive from the same direction. Differences can be seen in the RMS delay spread, power, NLoS error and coherence characteristics. Copyright © 2010 John Wiley & Sons, Ltd.

1. INTRODUCTION

Since the last decade, issues in wireless communication systems like the number of users and the demand for higher data rates are getting more and more critical. Therefore, it is essential to efficiently manage and utilise limited resources for future wireless network communication systems (e.g. Long Term Evolution (LTE)) [1]. Cognitive radio could act as an efficient allocator for frequency spectrum resources. Information about the locations of receiver and transmitter could further improve the system performance by enabling more optimal assignment of frequency resources to the crowded air channel. However, this aspect of how location information can benefit to communication systems has been rarely investigated, which has been demonstrated in Reference [1] to be useful. The fusion of positioning and communications are therefore gaining interests in research. Generally, location information can implicitly provide Channel State Information (CSI), like received power, Time of Arrival (ToA), Power Delay Profile (PDP), which may be used to adapt the modulation scheme, channel estimation or synchronisation inside the communication system to improve the overall performance.

Two well-known positioning techniques may be used to locate the receiver: (i) Fingerprinting (FIP) based positioning makes use of pre-collected CSI of the wireless channel saved in a database to find the best match to online measured values using a data recognition algorithm [2, 3]. (ii) Time Based (TB) positioning utilises the ranging information between transmitter and receiver to determine the target's location, where the range estimate is usually biased when the Line-of-Sight (LoS) signal is absent [4].

Both positioning and wireless communication strongly depend on the propagation channel. As one of the most challenging tasks, the indoor environment-based propagation channel in a femto-cell mobile radio environment is focused in this paper. Modern residential houses, office buildings and other constructions are usually multi-story buildings. Therefore, it is necessary to investigate channel characteristics of different floors in the same building. Several studies on the indoor to indoor multi-floors have been described in Reference [5]. This paper discusses the outdoor to indoor multi-floor channel characteristics for localisation and communication applications based on a channel measurement campaign at German Aerospace Center (DLR) premise in Oberpfaffenhofen.

* Correspondence to: Wei Wang, Institute of Communications and Navigation, German Aerospace Center (DLR), Oberpfaffenhofen, 82234 Wessling, Germany. E-mail: Wei.Wang@DLR.de
† A previous version of this paper was presented in the 7th International Workshop on Multi-Carrier System & Solutions (MC-SS 2009), Herrsching, Germany.

Received 19 March 2010
Accepted 30 March 2010

This paper is constructed as follows: in Section 2, the setup of the channel measurement campaign is addressed. Thereafter, Section 3 discusses the data processing methods and the evaluations. The corresponding channel characteristics comparison results are shown in Section 4 and conclusions are drawn in Section 5.

2. CHANNEL MEASUREMENT CAMPAIGN

The measurement was performed in a broadband Single Input Single Output (SISO) manner using the Medav RUSK-DLR channel sounder at operating centre frequency 5.2 GHz. The transmitter antenna was located on the rooftop of the office building TE02 of the Institute of Communications and Navigation (ICN) of DLR in a height of 12 m above ground. There the transmitter was emitting a 5 W chirp signal with a rectangular spectral shape of $B = 120$ MHz bandwidth. The transmitted periodic signal was vertically polarised with a period of 12.8 μs leading to to a maximum resolvable propagation distance of 3.84 km. The measured ith snapshot of the Channel Impulse Response (CIR), $h(i, j)$, $j = 0, \ldots, M-1$ consists of $M = 1537$ samples at delays $\tau_j = j\Delta\tau$, with $\Delta\tau = 1/B$. The discrete transfer function $H(i, m)$ contains the same number of samples at frequencies $m\Delta f$, $m = 0, \ldots, M-1$ with spacing $\Delta f \sim 78.125$ kHz. The channel sounder records one CIR every $T_g = 1.024$ ms providing a measurement rate of 976 CIRs per second (CIRs/s). The transmitter and receiver were synchronised by adjusting a 10 MHz Rubidium frequency normal at the receiver to the drifting of the transmitter frequency normal. Table 1 summaries the channel sounder setup for the measurements.

The receiver was located inside the office building TE01 of ICN with a spacing of 20 m between both buildings as visualised in Figures 1 and 2. The building itself can be characterised as a standard three story office building of concrete with metallised window glass. As our primary goal was to simulate a moving receiver instead of point measurements, the receiving antenna was mounted on a model train which is displayed in Figure 3, moving with a speed of $v \approx 0.15$ m/s. For the same transmitter position, the model train was running on the tracks $R1$ and $R2$, where $R1$ was fixed on the ground of the first floor (ground floor), and $R2$ on the second floor as shown in Figures 1 and 2. Both tracks $R1$ and $R2$ were located at the same positions relative to the building walls in the corridor, only differing in height above ground, to compare the channel characteristics for both floors.

Table 1. Channel sounder settings for the SISO measurement.

RF center frequency	5.2 GHz
Bandwidth B	120 MHz
Transmit power	5 W $\cong$ 37 dBm
Number of sub-carriers	1537
Measurement time grid T_g	1.024 ms
Antennas	Omni-directional (V)
Receiver speed v	0.15 m/s
Transmit height	12 m

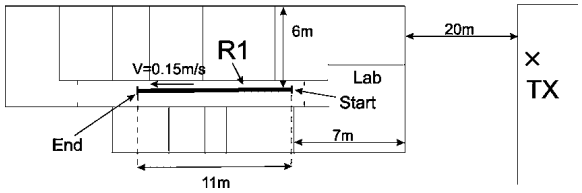

Figure 1. Track $R1$ on the first floor (ground floor) which runs through the corridor.

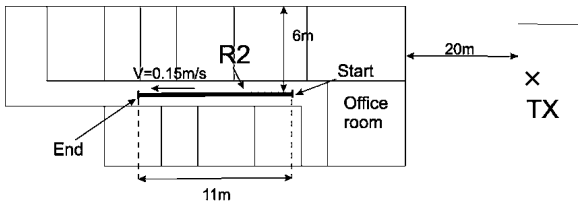

Figure 2. Track $R2$ on the second floor (3 m above ground floor) which runs through the corridor.

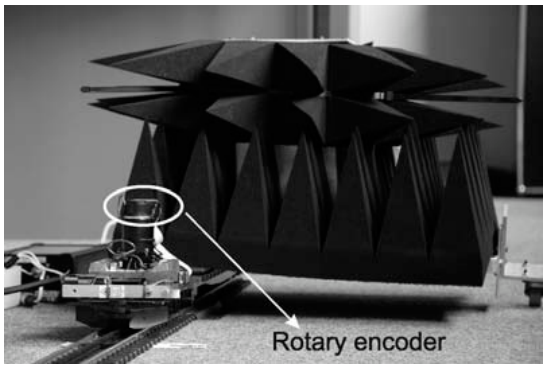

Figure 3. The model train used as mobile receiver platform shown without receiving antenna.

The position of the transmitter was precisely determined using a Leica tachymeter giving a nominal accuracy in the sub-cm domain. To get a similar accuracy for the receiver antenna mounted on the model train, the train is equipped with a rotary encoder giving 500 impulses per motor turn as described in Reference [6]. To prevent wheel slipping the model train runs by a cogwheel. Together with each CIR

DOI: 10.1002/ett

snapshot measurement $h(i, j)$ done in a periodic cycle of T_g the number of impulses given by the rotary encoder since movement start of the model train is saved, which results in a precise traveled distance measure for each captured impulse response snapshot. To validate the accuracy of the distance measurement by rotary encoder, $K = 21$ train runs have been performed. The K distance errors between estimated traveled distances $\hat{d}_i$ and the real distances d_i have a mean value of 0.16 mm/m and a standard deviation of 0.14 mm/m.

3. DATA PROCESSING AND EVALUATION

3.1. Channel characteristics evaluation

For wireless communication as well as for positioning, one of the most important measures of a wireless multipath channel is the PDP. Most common FIP positioning algorithms make use of the pre-measured received signal power or PDPs for an online pattern recognition [2, 3].

The PDP in this paper is denoted as $P(l, j)$ calculated as an average over normalised CIR snapshots $h_n(i, j)$ which are measured within a segment l of 0.2 m length on the model railway track. j denotes the delay bin of the sample at delay τ_j. $h_n(i, j)$ is the CIR snapshot $h(i, j)$ normalised in power by the maximum peak power and in delay as the CIR is shifted such that the first detected path above noise floor is at delay bin $j = 0$.

To obtain the RMS delay spread $\sigma_\tau(i)$ a threshold taken as the 99.9% quantile of a known noise region in $P(l, j)$ has been used. Unlike PDP, the RMS delay spread is not calculated segment by segment, but snapshot wise instead.

Frequency dispersion is usually measured by the coherence time. Using the traveled distance which is accurately measured by the odometer as described in Section 2, the coherence time can be expressed as the coherence distance $C_d(\rho)$ taking a constant speed of $v \approx 0.15$ m/s into account. A generic form of the auto-correlation for a specific series $\alpha(x)$ is given by Equation 1, where E_x denotes the expectation over x. For coherence distance in this paper, $\alpha(x)$ corresponds to the power amplitude $|H(i, m)|^2$, with distance $x = i \cdot v \cdot T_g$, and $\Delta x = \rho = k \cdot v \cdot T_g$ with $k = 0, 1, \ldots, W_D - 1$ and W_D stands for the number of CIR snapshots measurement while the train was running in the corridor. The correlation factor is calculated as the sample mean over frequency samples m. The coherence distance is usually regarded as the spatial correlation of the channel. Moreover, the value of CD_y is defined as the distance ρ where $C_d(\rho)$ falls to y% of the maximum.

To get an insight into the channel time dispersion characteristics, we calculate the coherence bandwidth $C_B(i, w)$ as the sample correlation of $H(i, m)$ with a spacing of $\Delta f = 78$ kHz. As a result, $C_B(i, w)$ can be calculated up to 60 MHz. To increase the signal to noise ratio, neighbouring 10 snapshots (≈ 1.4 mm), which are highly coherent, are averaged. Similar as Reference [7], the coherence bandwidth $C_B(i, w)$ for each CIR snapshot is calculated by Equation 1, where the $\alpha(x)$ is correspondingly the complex amplitude of frequency $H(i, m)$, $x = m$ and $w = \Delta x = k \cdot \Delta f$ with $k = 0, 1, \ldots, M - 1$. The coherence bandwidth is calculated for each snapshot i. Similar as coherence distance, the value of $\mathrm{CB}_y(i)$ is defined as the bandwidth w where $C_B(i, w)$ falls to y% of the maximum.

As another channel characteristic, the None Line-of-Sight (NLoS) error is important for TB positioning [6, 8] defined as the difference of propagation distance of the first detectable path to the Geometric Line-of-Sight (GLoS). The GLoS delay $\mathrm{ToA}^{\mathrm{GLoS}}(i)$ is determined by the measured distance between transmitter and receiver divided by the speed of light. For NLoS scenarios the first detectable incoming path has a greater propagation distance than the GLoS resulting in a bias for ranging applications. The NLoS error $\varepsilon_{\mathrm{NLoS}}(i)$ for snapshot i is defined by

$$\varepsilon_{\mathrm{NLoS}}(i) = c \cdot (\mathrm{ToA}^{\mathrm{FP}}(i) - \mathrm{ToA}^{\mathrm{GLoS}}(i)), \tag{2}$$

where $\mathrm{ToA}^{\mathrm{FP}}(i)$ is the estimated delay of the first incoming path and c denotes the speed of light. To evaluate the coherence characteristics of the NLoS error, the spatial correlation of NLoS error $C_\varepsilon(\rho)$ is calculated by Equation 1, where the $\alpha(x)$ corresponds to the NLoS error $\varepsilon_{\mathrm{NLoS}}(i)$, $x = i \cdot v \cdot T_g$ and $\rho = \Delta x$.

3.2. Virtual antenna array (VAA) processing

Generally, estimation of Angle of Arrival (AoA) information with antenna array takes the benefits of incoming phase

$$C(\Delta x) = \frac{E_x\{(\alpha(x) - E_x\{\alpha(x)\})(\alpha(x + \Delta x)^* - E_x\{\alpha(x + \Delta x)^*\})\}}{\sqrt{E_x\{(\alpha(x) - E_x\{\alpha(x)\})^2\} E_x\{(\alpha(x + \Delta x)^* - E_x\{\alpha(x + \Delta x)^*\})^2\}}} \tag{1}$$

DOI: 10.1002/ett

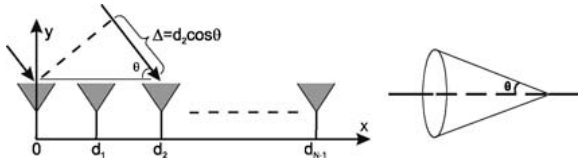

Figure 4. 1D AoA estimation with linear antenna array based on signal phase difference between neighbouring antenna elements.

differences for different antenna elements. Figure 4 gives an example of a linear array to estimate the incoming 1D AoA. As described in Section 2, the measurement was performed in the SISO manner with single antenna which does not provide spatial phase difference information. However, it is possible to extract the linear antenna array from the measurement due to the utilisation of rotary encoder. The distance error per metre estimated through the odometer measurement is 0.16 mm/m in average which is small enough to be ignored according to Section 2, which makes it possible to form a linear VAA as shown in Figure 5. In this paper, the train movement direction along the corridor is defined as the x-axis in Figure 4, meaning that for the receiver antenna positioned at the end of the track a ray coming from the start point of the track has a AoA of 0°.

3.3. Channel parameters estimation with SAGE

To accurately obtain the $\mathrm{ToA}^{\mathrm{FP}}(i)$ from the bandlimited CIR, the Space-Alternating Generalised Expectation-maximisation (SAGE) super resolution algorithm [9, 10] has been utilised to estimate the path delays, amplitudes, phases and the AoA from the measured raw data. Without loss of generality, the received signal can be denoted as the summation of paths plus additive noise $\mathbf{n}(i, j)$

$$\mathbf{h}(i, j) = \sum_{l=1}^{L(i)} \mathbf{x}_l(i, j) + \mathbf{n}(i, j) \tag{3}$$

where $\mathbf{h}(i, j) = \big[h(i, j), \ldots, h(i + N - 1, j)\big]$ with the number of antenna elements N and $\mathbf{x}_l(i, j) = \mathbf{a}(\theta_l(i))\alpha_l(i)s(j - \tau_l(i) \cdot B)$. $\mathbf{a}(\theta_l(i))$ denotes the steering vector, $\theta_l(i)$ is the 1D AoA, $\alpha_l(i)$ the complex amplitude of path l, $\tau_l(i)$ the delay of path l and $s(j)$ denotes the transmitted reference signal which is a dirac function within the bandwidth. $\hat{\Theta}_l(i) = [\hat{\tau}_l(i), \hat{\theta}_l(i), \hat{\alpha}_l(i)]$ is the parameter vector to be estimated and $L(i)$ is the number of paths for snapshot i which is estimated by Minimum Description Length (MDL) [11]. Starting from initialisation value, the parameter could be obtained iteratively by the maximisation step following the expectation step which estimates the hidden data space with $\mathbf{r}_l(i, j) = \mathbf{h}(i, j) - \sum_{k=1}^{l-1} \mathbf{x}_k(i, j)$. In this paper 2D-SAGE is considered with steering vector $\mathbf{a}(\theta) = [1, e^{-j2\pi \frac{d_1}{\lambda} \cos\theta}, \ldots, e^{-j2\pi \frac{d_{N-1}}{\lambda} \cos\theta}]^T$, where d_n is the spacing between the nth element and the element '0' as shown in Figure 4.

4. EVALUATION RESULTS OF CHANNEL CHARACTERISTICS

4.1. PDP and RMS delay spread

The Probability Density Functions (PDFs) of the PDPs $P(l, j)$ for track $R1$ on the first floor and track $R2$ on the second floor are presented in Figures 6 and 7. As clearly visible the PDPs for both floors have a 'two-cluster' structure, starting with the fist cluster at 0 μs and the second at approximately 0.15 μs. The delay gap between both clusters results in an equivalent propagation distance of approximately 45 m. The second cluster is most probably caused by outdoor reflections between both buildings which are 20 m spaced as shown in Figures 1 and 2. The windows of the buildings are metallised and do have therefore good electromagnetic reflection properties.

For the first floor, the electromagnetic waves are most probably propagating through the lab, which is directed towards the transmitter as shown in Figure 1, before arriving at the antenna placed in the corridor. However, for the second floor, the amplitude of the waves suffer from additional

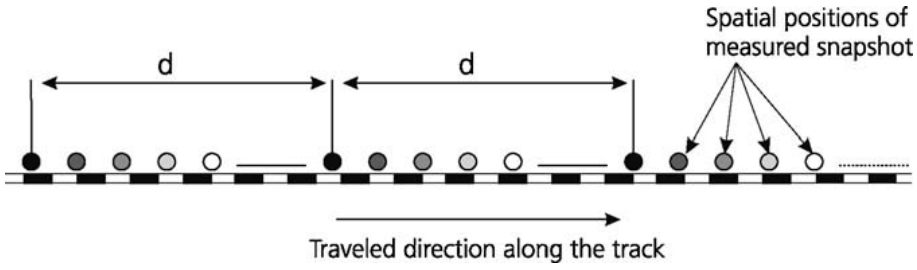

Figure 5. VAA generation in the measurement.

DOI: 10.1002/ett

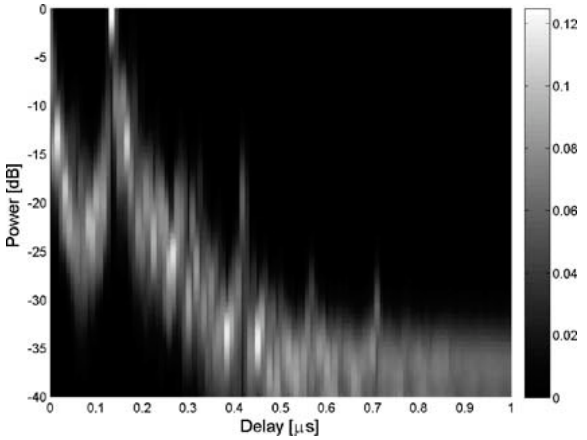

Figure 6. PDF estimate for $P(l, j)$ taken while the model train is running on track $R1$. A Gaussian kernel estimator [12] has been used to estimate the one-dimensional PDF of $P(l, j)$ at each delay bin j.

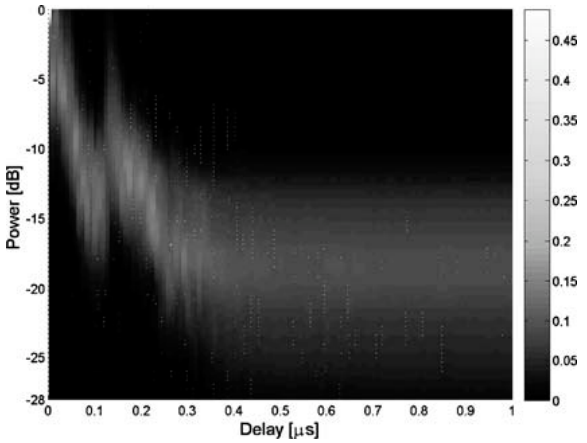

Figure 7. PDF estimate for $P(l, j)$ taken while the model train is running on track $R2$. A Gaussian kernel estimator [12] has been used to estimate the one-dimensional PDF of $P(l, j)$ at each delay bin j.

transmission loss compared to the first floor due to the office rooms located at the outer wall directed towards building TE02. Therefore, the power received when the model train runs on $R1$ is larger than the power obtained when running on $R2$ as shown in Figure 8.

Although the PDPs of both tracks share the same cluster structure, in the first floor the second cluster has a higher mean value in power compared to the first cluster, whereas in the second floor the first cluster has a higher probability for a higher power level compared to the the second cluster. The RMS delay spread values listed in Table 2 can be explained by the PDPs of the different floors. For the track $R1$, the power is more focused on the second cluster, while for track $R2$, the power is mostly focused on the first cluster. As a result, the RMS delay spread obtained from measurements for track $R1$ is larger than the delay spread obtained for measurements on $R2$.

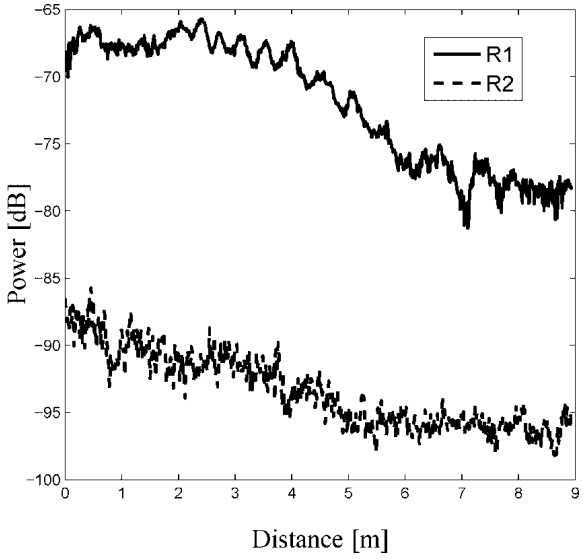

Figure 8. Received power in dB when receiver was running along both tracks.

Table 2. Statistical parameters of RMS delay spread, μ denotes the mean value and σ stands for the standard deviation.

	$R1$	$R2$
μ (ns)	64.7438	39.6660
σ (ns)	12.4343	21.3655

4.2. Coherence distance and coherence bandwidth

The coherence distance computed according to Section 3 is decreasing fast with distance ρ for both tracks as shown in Figure 9. The CD_{50} of track $R1$ and $R2$ are 24.39 and 1.47 cm, respectively, while for CD_{90} value of 0.9 and 0.19 cm are obtained. The coherence distance calculated when running on $R1$ is higher compared to the value associated with $R2$. As the coherence distance with respect to CD_{50} along the corridor is rather small, $|H(i, m)|^2$ is less correlated over spatial distance as the receiver moves along the corridor. The FIP based position algorithms could benefit from this due to less dependence of features, like PDPs, for neighbouring points.

The coherence bandwidth information is essential for communication systems. For instance, for orthogonal frequency division multiplexing systems, the frequency spacing should be less than the coherence bandwidth and the symbol time is less than the coherence time. Figures 10

DOI: 10.1002/ett

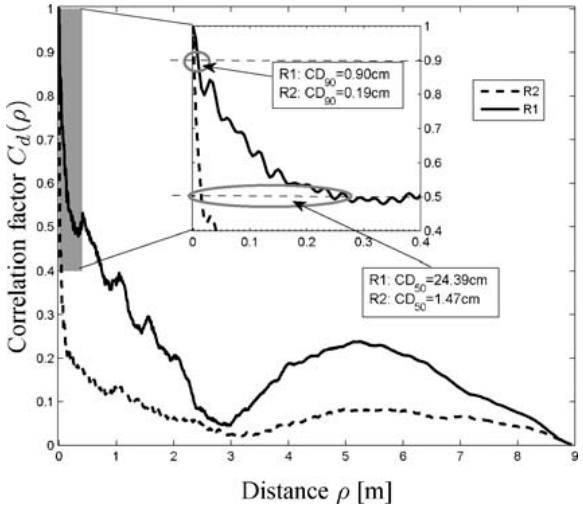

Figure 9. Spatial correlation properties of CIRs at different floors.

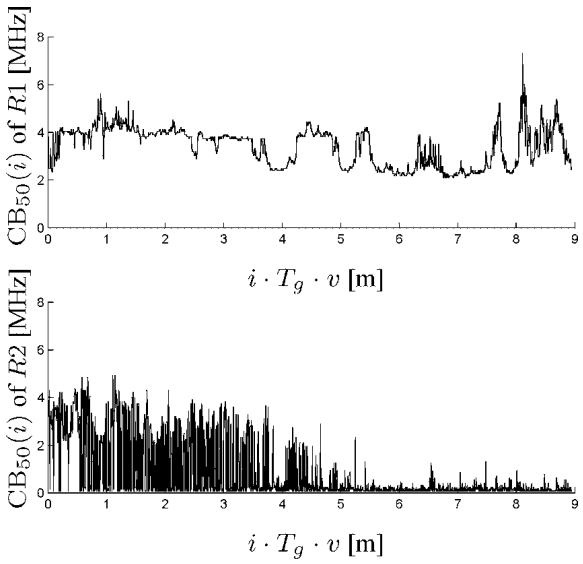

Figure 10. Coherence bandwidth referring to a correlation of 50% when the receiver was running on tracks.

and 11 show the computed coherence bandwidth referring to correlation levels $CB_{50}(i)$ and $CB_{90}(i)$ for the received signal while the model train was running on the tracks. The coherence bandwidth keeps almost constant as the receiver moves on $R1$ further into the corridor referring to correlation level of 50% and 90%. When running on $R2$, the coherence bandwidth referring to 50% keeps constant and decreases as the receiver moves further after 5 m into the corridor, whereas the coherence bandwidth referring to 90% keeps constant from 1.5 to 5 m. Thereafter the coherence bandwidths drop down to a small value. This can be explained by the fact that, the received power in the parts after 5 m

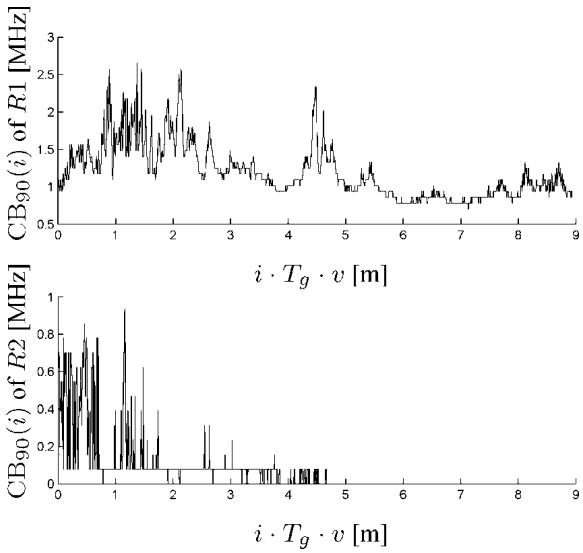

Figure 11. Coherence bandwidth referring to a correlation of 90% when the receiver was running on tracks.

Table 3. Statistical parameters of coherence bandwidth, μ denotes the mean value and σ stands for the standard deviation.

	μ (MHz)	σ (MHz)
$R1$, $CB_{50}(i)$	3.40	0.80
$R1$, $CB_{90}(i)$	1.19	0.35
$R2$, $CB_{50}(i)$	0.86	1.27
$R2$, $CB_{90}(i)$	0.07	0.14

of $R2$ are small so that the correlations are more affected by noise. The statistical parameters of the coherence bandwidth are listed in Table 3.

4.3. Number of paths, delay and AoA

The results of detected number of paths for CIRs measured while the train was moving on track $R1$ and $R2$ using MDL are depicted in Figure 12. The difference in the quantity of paths detected for both floors indicates the significant influence of building structure on the outdoor to indoor propagation channel. For the second floor the office room located at the wall towards building TE02 introduces significantly more attenuation such that more paths are below the noise floor and cannot be detected any more.

As another important measure the AoA of a path provides geometric information of propagation mechanism, which is usually utilised in a statistical analysis like a joint AoA-delay probability density function. Figures 13 and 14 show the joint distribution for the estimated channel parameters using a VAA as described in Section 3.2. Similar to the

DOI: 10.1002/ett

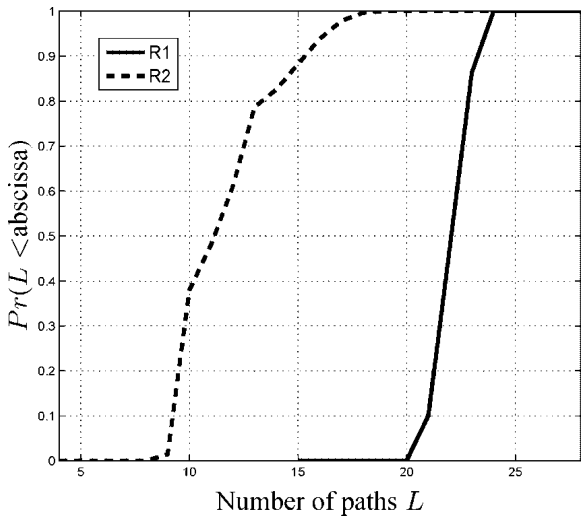

Figure 12. Cumulative density function of detected number of paths by MDL for both tracks.

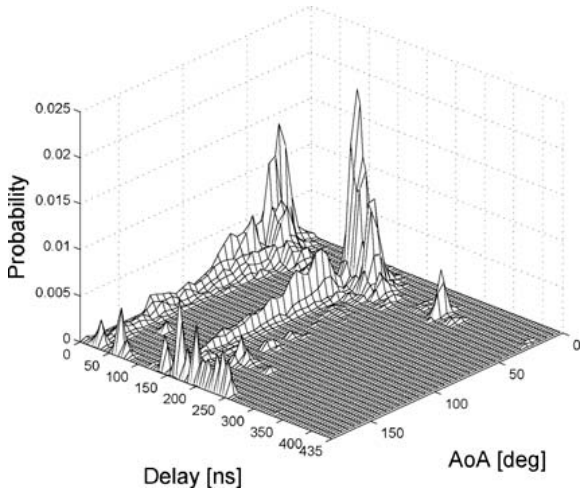

Figure 13. Joint AoA-delay PDF of measurements taken while the train was running on track $R1$.

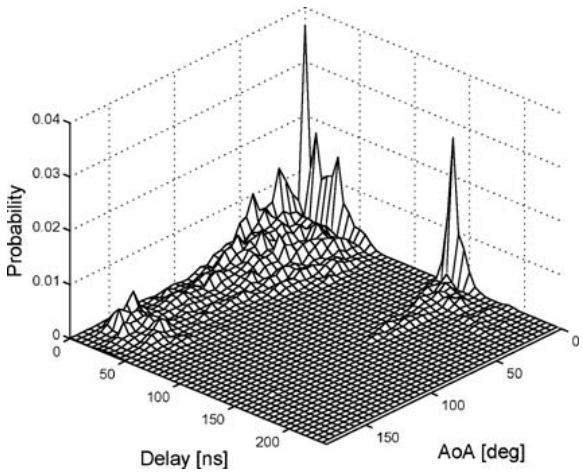

Figure 14. Joint AoA-delay PDF of measurements taken while the train was running on track $R2$.

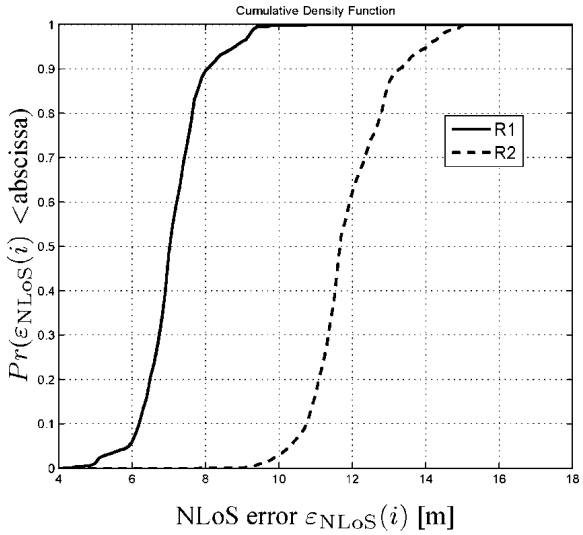

Figure 15. Cumulative density function of NLoS errors $\varepsilon_{\mathrm{NLoS}}$.

results obtained for PDPs, two clusters in delay domain with similar AoAs are visible. The second cluster located at $\tau_j \approx 150$ ns after the first one, which equates to an additional propagation distance of 45 m. This confirms the conclusions in Section 4.1, that reflections between two buildings introduce the second cluster as rays from both clusters are arriving with a similar AoA.

For measurements taken on track $R1$ on the first floor most incoming rays are from a direction lying on a cone with an opening angle of $\sim 30\,^\circ$. However, for track $R2$ on the second floor, the paths are mostly from $\sim 0\,^\circ$ direction.

Figure 15 shows the Cumulative Density Function (CDF) of estimated NLoS errors $\varepsilon_{\mathrm{NLoS}}(i)$ for measurements performed on both tracks $R1$ and $R2$. From the CDF it can be noticed that for the values obtained from measurements on the second floor are larger than on the first floor, which can be explained through the additional attenuation caused for the GLoS and rays with a similar propagation path due to the office rooms.

The corresponding spatial correlations for the NLoS errors on both floors are given in Figure 16, where it is noticeable that the NLoS error calculated for measurements performed on the second floor has a larger correlation distance compared to the ones for the first floor. In other words, the NLoS error varies slower for measurements over distance on the second floor. The AoA information of the first detectable path provides more insides into the NLoS errors. Figures 17

DOI: 10.1002/ett

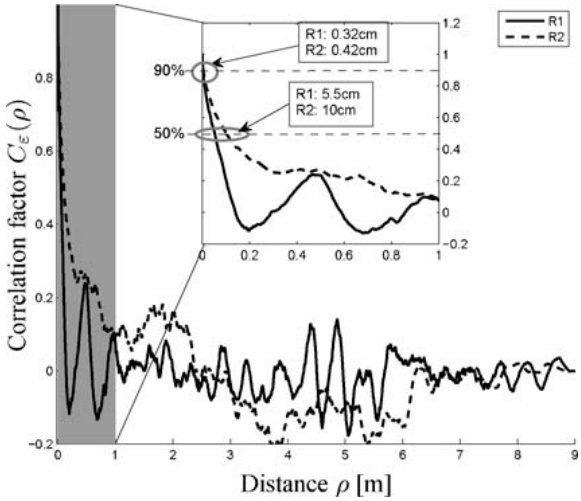

Figure 16. Spatial correlation properties of NLoS error $\varepsilon_{\mathrm{NLoS}}$ at different floors.

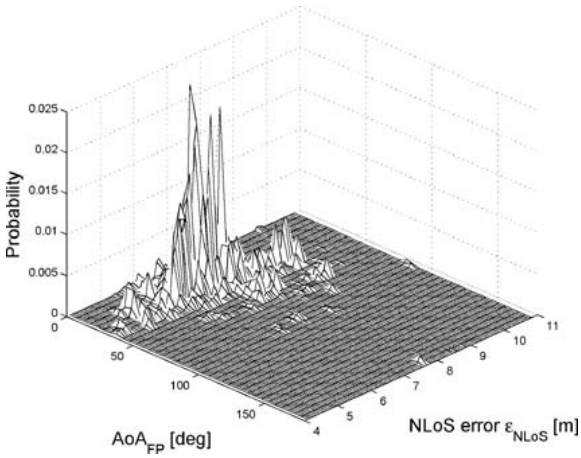

Figure 17. Joint $\mathrm{AoA_{FP}}$-$\varepsilon_{\mathrm{NLoS}}$ PDF of measurement with $R1$.

and 18 show the joint $\mathrm{AoA_{First\ path}}$-$\varepsilon_{\mathrm{NLoS}}(i)$ PDFs obtained for measurements on both tracks. According to Figure 18, the first detectable incoming paths are mostly arriving from the direction of the transmitter.

5. CONCLUSION

In this paper, based on an outdoor to indoor broadband wireless channel measurement campaign for femto-cell mobile radio environment, we addressed the channel characteristics and a comparison between signals received on two different floors to study the wireless channel for communications and localisation applications. The propagation characteristics are presented in terms of PDPs, coherence distance,

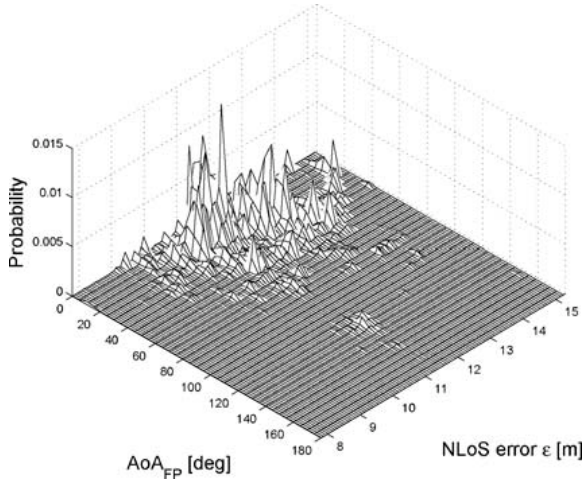

Figure 18. Joint $\mathrm{AoA_{FP}}$-$\varepsilon_{\mathrm{NLoS}}$ PDF of measurement with $R2$.

coherence bandwidth, RMS delay spread, AoA and NLoS error. The evaluation shows for these measurements that CIRs measured on both floors have PDPs with a two-clusters structure where the first cluster is caused by direct propagation into the building and the second cluster is caused by the reflections between two buildings. The obtained coherence distances are small, which indicates that CSIs are nearly independent over short distance for both floors. This is an advantage for FIP positioning as the feature should be as discriminant as possible. Moreover, the estimated AoAs show that paths are mostly arriving from the transmitter direction in both floors. However, the RMS delay spread, the coherence bandwidth and NLoS error are different from floor to floor. In general, all results measured are reflecting the building and its surroundings in terms of wave propagation which could be used for channel modelling. Nevertheless for similar environments channel characteristics can be expected alike the ones described.

ACKNOWLEDGEMENTS

This work was co-founded by DLR internal project Galileo ADvanced APplications (GalileoADAP) and the European Community's Seventh Framework Programme FP7-ICT-2007-1 under contract number 217033 referred as Wireless Hybrid Enhanced Mobile Radio Estimators (WHERE).

REFERENCES

1. Raulefs R, Plass S. Combining Wireless Communications And Navigation — The WHERE Project. In *Proceedings of 68th IEEE Vehicular Technology Conference (VTC 2008-Fall)*, Calgary, September 2008.

2. Bahl P, Padmanabhan V. RADAR: An In-Building RF-based User Location and Tracking System. In *Proceedings of INFOCOM 19th Annual Joint Conference of the IEEE Computer and Communications Societies. IEEE.* 2000; **2**: 775–784.
3. Triki M, Slock D, Rigal V, Francois P. Mobile Terminal Positioning via Power Delay Profile Fingerprinting: Reproducible Validation Simulations. In *Proceedings of 64th IEEE Vehicular Technology Conference (VTC 2006-Fall)*, Montreal, Canada, 2006.
4. Sayed AH, Tarighat A, Khajehnouri N. Network-Based Wireless Location: challenges faced in developing techniques for accurate wireless location information. *IEEE Signal Processing Magazine* 2005; **22**:24–40.
5. Lott M, Forkel I. A Multi-wall-and-floor Model for Indoor Radio Propagation. In *Proceedings of the 53rd IEEE Vehicular Technology Conference (VTC 2001-Spring)*, Rhodes, Greece, March 2001.
6. Jost T, Wang W. Satellite-to-Indoor Broadband Channel Measurements at 1.51 GHz. In *Proceedings of the ION International Technical Meeting (ITM)*, Anaheim, California, January 2009.
7. Gligorevic S, Zierhut R, Jost T, Wang W. Airport Channel Measurements at 5.2 GHz. In *Proceedings of the 3rd European Conference on Antennas and Propagation (EuCAP)*, Berlin, Germany, March 2009.
8. Wang W, Jost T, Mensing C, Dammann A. ToA and TDoA Error Models for NLoS Propagation Based on Outdoor to Indoor Channel Measurement. In *Proceedings of the IEEE Wireless Communications and Networking Conference (WCNC) 2009*. Budapest, Hungary, April 2009.
9. Fleury B, Tschudin M, Heddergott R, Dahlhaus D, Pedersen K. Channel parameter estimation in mobile radio environments using the SAGE algorithm. *IEEE Journal on Selected Areas in Communications* 1999; **17**(3):434–450.
10. Chong CC, Laurenson DI, McLaughlin S. Joint detection-estimation of directional channel parameters using the 2-D frequency domain SAGE algorithm with serial interference cancellation. *In Proceedings of IEEE International Conference on Communications* 2002; **2**:906–910.
11. Xu G, Roy RH, Kailath T. Detection of number of sources via exploitation of centro-symmetry property. *IEEE Transactions on Signal Processing* 1994; **42**(1):102–112.
12. Silverman BW. *Density Estimation for Statistic and Data Analysis*. Chapman and Hall, New York, NY, 1986.

DOI: 10.1002/ett

A.4 Introduction of a Time-variant Component Related to Human Activity Into WINNER 2 Model

Wireless time-variant stochastic channel model including the human activity for indoor positioning

Yoann Corre, Julien Stéphan, Mathieu Brau,
Radio Department
SIRADEL S.A.S.
Rennes, France
ycorre@siradel.com

Yves Lostanlen
Wireless Expertise and Research Center
SIRADEL
Toronto, Canada
yves.lostanlen@ieee.org

Abstract—**A time-variant wireless stochastic channel model for indoor transmitter is proposed in this paper. Time-variant components taking into account the human activity are introduced into geometry-based stochastic channel predictions. The proposed model aims at feeding evaluation of indoor geolocation algorithms with realistic non-stationary characteristics for wireless systems serving indoor areas. The model formulation is generic, and has been adjusted to static line-of-sight links within corporate environments at a central frequency 2GHz.**

Stochastic channel modelling; time-variant channel; indoor geolocation; human activity; fixed indoor radio link;

I. INTRODUCTION

The human activity strongly influences the wireless channel properties in indoor environments: the received signal strength (RSS) is attenuated in populated areas (e.g. office, residential building, shopping mall); the temporal variability of the time of arrival (ToA) or the time differences of arrival (TDoA) as well as the dispersion on the angles of arrival (AoA) are amplified by obstruction or scattering by people motion around the main propagation paths. These impacts are expected to be more significant on radio links with low antenna configuration.

Realistic positioning approaches for indoor environments need to consider fading caused by the movement of people or the presence of furniture. The model proposed in this paper aims at providing channel simulations of indoor transmitter deployments including the human activity. The method basically consists in introducing a time-variant contribution into a geometry-based stochastic channel prediction, taking into account the path geometries and the random distribution of human bodies.

Only few channel models have been designed in order to provide realistic estimation of geolocation techniques performance. In [4], the authors propose a two-level channel model based on an extension of the CODIT model. More recently, a channel model based on statistical modeling approach for ToA, AoA and amplitude of the multipath components was proposed [5]. Nevertheless, these models do not fully account for the impact of human activity in indoor environment. Besides, different methods were used in the literature to establish a channel model that takes account this effect. Multi-state Markov chain is the most frequently proposed solution. In multi-state Markov chain model, transition probabilities and the values of factor K for different states are two crucial parameters. For example, the authors of [7] make use of [6] measurements to construct a two-state Ricean model where the periods with very low fading (K-value between 10 and 12dB) are distinguished from periods with severe fading (K-value=0dB, i.e. Rayleigh distribution). The model is simulated with a two-state Markov process associated to transition probabilities p and q for respectively transition to severe fading and transition to low fading.

CW Measurements reported in [6] were conducted at the frequency 910MHz in two kinds of office environments. In building 1, one terminal is located in a small room whereas the other terminal is located in a long corridor. The fading related to human activity and "machinery" occurs in bursts of tens of seconds in duration, with 30dB dynamic range. In building 2, both terminals are located in the same large open space. The fading is more continuous with 17dB dynamic range. In most cases, the Ricean distribution is found to fit well to the power distribution during fading occurrence, with K-value in the range 6dB to 12dB. Besides, ITU-R P.1238 [1] show that the fading related to human activity is bursty and the channel statistics present some strong non stationarities. Measurements at 1.7GHz indicate that a person moving into the path of a LOS (Line-Of-Sight) signal causes a 6 to 8dB drop in received power level, and the K-value of the Nakagami-Rice distribution is considerably reduced. In the case of non-LOS conditions, people moving near the antennas did not have significant effects on the channel properties.

Based on their observations, ITU-R P.1238 suggest an analytical model for static LOS and NLOS radio links, where indirect paths arrive at the MD (Mobile Device) with uniformly distributed horizontal directions, and persons are moving in random directions with constant speed. The received power is modelled by the Nakagami-Rice distribution with K-values depending on the number of moving persons, the room size and the direct/indirect power ratio. The autocorrelation function and Doppler power spectrum of the received power are defined as well to characterise continuous time variations. This approach provides time-variant received powers and it does rely on a uniform distribution of path directions. However it is not suited to be integrated into a stochastic geometry-based channel model.

The TGn models from IEEE 802.11 [2] associate a non-zero Doppler power spectrum to the taps representing the delayed channel components, then allowing the simulation of temporal fluctuations in power level. This Doppler power spectrum is given by $S(f) = (1 + 9\,(f/f_d)^2\,)^{-1}$, where $S(f)$ is a Bell shape function, expressed in linear, and f_d was experimentally found to be around 3Hz at 2.4GHz.

The stochastic geometry-based WINNER 2 [3] model may associate some channel multi-paths to moving persons or scatterers, in indoor and microcell outdoor- indoor scenarios. The reflection is assumed to be the main interaction with human body in the targeted frequency range 2GHz – 6GHz. The procedure is roughly as follows: the channel properties are predicted for the fixed link; then a given percentage of clusters are assumed to be related to moving clusters; the number of rays within the cluster being generated by a moving scatterer is determined from the target temporal K-value; the mean velocity and direction of the moving clusters are simulated in a random way; then the Doppler frequency of the impacted rays is calculated from the ray geometry, the cluster velocity and direction. This procedure is partly reused in the solution proposed in this paper, however the main interaction is assumed to be shadowing whereas scattering is neglected.

A more precise approach is proposed in [8]. It is based also on a two-state Ricean model, but the calculation of the fading depends on the geometry: distance between radio terminals, distance between the person and the terminals, height of terminal antennas, height of the person. The model deals with the obstruction of the LOS direct path and assumes that the main impact of persons is diffraction; actually the person is considered as an absorbing screen. The fading is predicted from a three-knife-edge-diffraction method, i.e. from the sum of the three following components: knife diffraction at one edge of the human body; knife diffraction at the other edge; and knife diffraction by the top edge of the human body. The validity of this three-knife-edge-diffraction method is proven by comparison to CW measurements at 2.4GHz with controlled person movements.

Besides, ray-tracing models may be combined with a physical human body representation (e.g. a cylinder filled by salty water [9]) to generate site-specific interactions between the persons and the wave propagation or to extract statistics on the channel variations.

Some of these results are exploited in the solution described in this paper, leading to introduction of a time-variant component into Geometry-based Stochastic Channel Models (GSCM), and WINNER 2 model in particular. The remaining is divided as follows. Section II describes the elaborated solution. Section III discusses the parameterization of this time-variant contribution. Finally, section IV gives first simulation results. This work was conducted in the context of indoor geolocation, then the radio terminals are referred as AP (access point) and MD (mobile device).

II. TIME-VARYING CHANNEL PREDICTION

A. *General principles*

The time-variant channel model described in this section predicts multi-path channel properties for a static SISO radio link that undergoes variations due to human body obstructions. The whole process depicted in Fig. 1 generates continuous channel realizations that result from correlated "human activity snapshots".

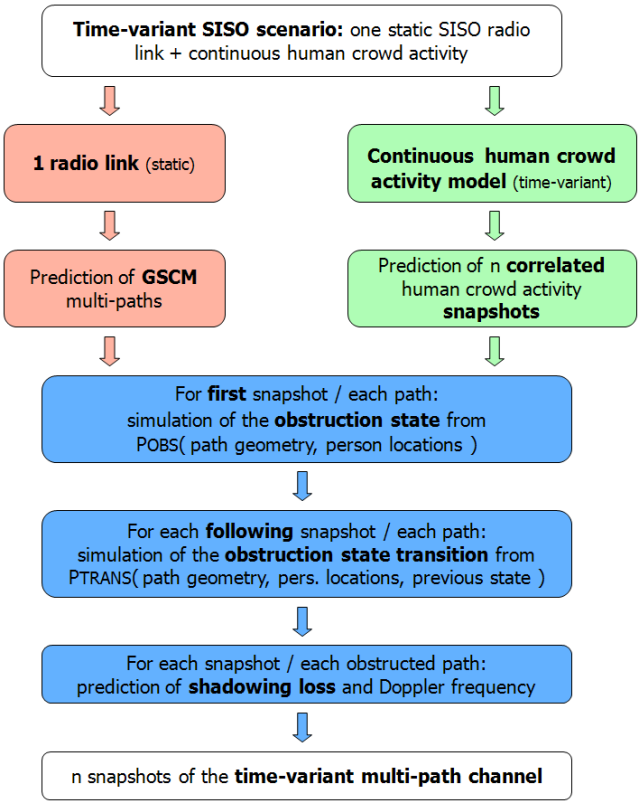

Figure 1. Process for time-variant GSCM predictions.

On one hand, the static SISO radio link is defined by the AP and MD locations; AP and MD single antenna properties (pattern and orientation); and central propagation frequency, All these parameters are injected into the GSCM model to get the static multi-path channel prediction. On the other hand, the human activity model defines statistical characteristics of the person locations. Statistics on the person density is sufficient when the prediction does not care about time-continuity. Otherwise, a velocity and mobility path (possibly random) is associated to each person to provide time-correlated snapshots of person distributions. Finally, the time-variant channel prediction is obtained from each human activity snapshot. At the I^{th} snapshot, the number of obstructions of each path PT_J is simulated, depending on the person locations $PE_{I,K}$ and the path geometrical properties given by the GSCM model.

WINNER 2 is the considered GSCM model in this paper. The predicted path geometrical properties are: path-length; departure horizontal angle; departure vertical angle; arrival horizontal angle; arrival vertical angle. The exact trajectory of indirect paths (i.e. paths that undergo at least one interaction

with the environment) is unknown. Only the LOS direct path is perfectly known, when existing, thus the simulation of its "obstruction state" is done in a specific way.

B. *Simulating the obstruction state of indirect paths*

At the first predicted snapshot, the probability that the person $PE_{I,K}$ obstructs the path PT_J is given by the following obstruction probability function:

$$p1(PE_{I,K}, PT_J) = f(\Delta l, dh_1, dv_1, \phi_1, \theta_1, dh_2, dv_2, \phi_2, \theta_2) \quad (1)$$

where Δl is the excess path-length defined as the difference between the path-length and the AP - $PE_{I,K}$ - MD length; dh_1 (resp. dh_2) is the horizontal distance between AP (resp. MD) antenna and the person location; dv_1 (resp. dv_2) is the minimum vertical distance between AP (resp. MD) antenna and the person location; ϕ_1 (resp. ϕ_2) is the horizontal angle difference between the AP path direction and the direction from AP to the person location; and θ_1 (resp. θ_2) is the minimum vertical angular difference between the AP path direction and the direction from AP to the person location. Remark that $p(PE_{I,K}, PT_J) = 0$ when $\Delta l < 0$m.

The obstruction of the path PT_J by the person $PE_{I,K}$ is simulated from the two-state random variable $S_{I,J,K}$ with obstruction probability $p1(PE_{I,K}, PT_J)$.

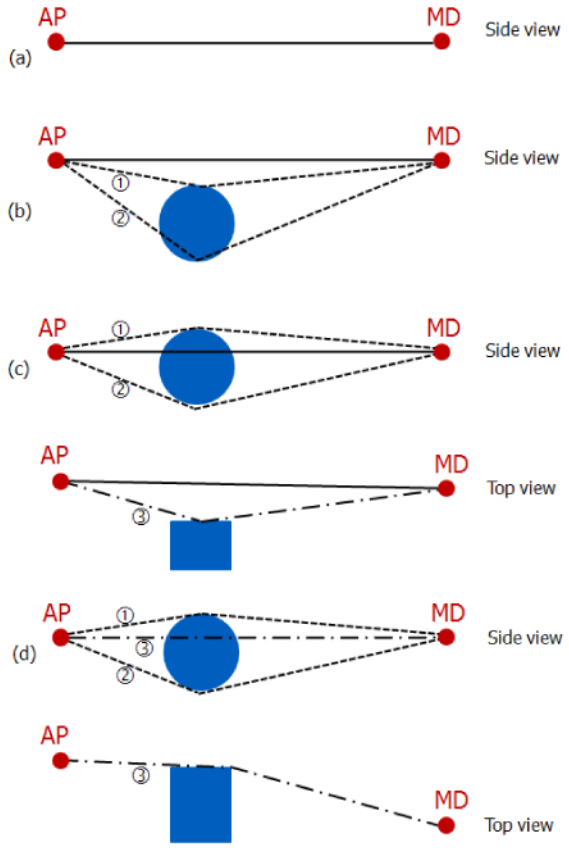

Figure 2. Multi-paths involved in the LOS obstruction.

At following snapshots, the probability that the person $PE_{I,K}$ obstructs the path PT_J depends on the previous obstruction state and state duration:

$$p2(PE_{I,K}, PT_J) =$$

$$g(\Delta l, dh_1, dv_1, \phi_1, \theta_1, dh_2, dv_2, \phi\$_2, \theta_2, S_{I\text{-}1,J,K}, \delta_{I,J,K}) \quad (2)$$

where $PE_{I\text{-}1,K}$ is the person location at the previous snapshot; $S_{I\text{-}1,J,K}$ is the obstruction state at the previous snapshot; and $\delta_{I,J,K}$ is the distance covered by the person from the last change in obstruction state up to the current snapshot.

A unique 7dB attenuation is applied to each obstructed path, compliant to the 6-8dB attenuations reported by [1].

A random non-zero Doppler shift is simulated to each obstructed path, with a probability density function (PDF) similar to the Bell-shaped Doppler power spectrum given in [2] at 2.4GHz. The Doppler shift is assumed to be constant during the whole obstruction.

C. *Simulating the obstruction state of the LOS direct path*

The geometry of the LOS direct path is fully known. Thus its power variations may be predicted in a very realistic way. The method described below is inspired from [8], and some enhancements permit to deal with a larger number of person distribution cases (especially when nobody obstruct the direct path) and determine a Doppler shift.

As shown in Fig. 2, four different situations are distinguished when only one person is within the propagation environment:

(a) The person is not in the vicinity of the LOS direct path. The LOS direct path is unchanged, with zero Doppler shift.

(b) The person is approaching the LOS direct path, but does not yet obstruct the line-of-sight. Two indirect paths, diffracted at ① the interior edge and ② the exterior edge of the person, are assumed to interfere with the direct path. The LOS direct path is replaced by two contributions:

- The first contribution has similar geometrical properties than the direct path, except that the propagation loss accounts for the additional knife-edge diffraction loss L_{KF1} that results from diffraction at the interior edge of the person and oscillates around 0dB.
- The second contribution is the diffracted path represented by the trajectory ①. The propagation loss is the direct path loss plus the knife-edge diffraction loss L_{KF2} > 6dB resulting from diffraction at the exterior edge of the person. This second contribution is negligible when the person is far away from the line-of-sight obstruction, but becomes more significant when the person is approaching. This second contribution is associated to a non-zero Doppler shift, which is simply calculated from the phase shift related to the path length variations when the person is moving.

(c) The person is crossing the horizontal projection of the line-of-sight, but the line-of-sight passes above the person head. Three indirect paths, diffracted at ① the interior edge, ② the exterior edge and ③ the head of the person, are assumed to interfere with the direct path. The LOS direct path is replaced by three contributions:

- The first contribution has similar geometrical properties as the direct path, except that the propagation loss accounts for the additional knife-edge diffraction loss L_{KF3} that results from diffraction above the head of the person and oscillates around 0dB.
- The other contributions are the diffracted paths represented by trajectories ① and ②. The propagation loss is the direct path loss plus the knife-edge diffraction loss L_{KF1} and L_{KF2} respectively, both of them > 6dB. These contributions are associated to non-zero Doppler shifts.

(d) The person is crossing the line-of-sight. The direct path is assumed to be negligible. It is replaced by three indirect paths:

- The first contribution is the diffracted path represented by the trajectory ③. The propagation loss is the direct path loss plus the knife-edge diffraction loss L_{KF3} > 6dB. This contribution is associated to a non-zero Doppler shift.
- The other contributions are similar to those of case (c).

The algorithm becomes more complex when several persons are in the vicinity of the LOS direct path. It has been decided to preserve the same multi-path construction as illustrated in Fig. 2, with following adjustments:

(b-extended) Several persons are around the LOS direct path, but there is no obstruction. Path ① is constructed from the person that generates the highest diffraction loss. Path ② is constructed from the shortest unobstructed trajectory diffracted at the exterior edge of a person, on the same side than path ①.

(c-extended) and (d-extended) At least one person obstructs the LOS direct path. Path ① and Path ② are constructed on each side of the LOS path from the shortest unobstructed trajectories diffracted at the exterior edge of a person.

With this approach, the algorithm deals with more than one person in the propagation environment, but this has to be evaluated or further adjusted.

III. MODEL PARAMETERIZATION

The stochastic time-variant channel model relies on an obstruction probability function and an obstruction transition probability function, which have to be as close as possible to reality. These probability functions could be empirically derived from a large set of channel measurements associated to controlled person movements. However this approach is very costly in terms of time, resource and measurement processing. That is why, to feed the model with realistic values, 3D ray-tracing predictions [10] are preferred to generate reference data.

The purpose is to derive obstruction probabilities related to the geometrical path parameters used in section II, by analysing a large number of path-person pairs, where paths are simulated by the ray-tracing and persons are uniformly distributed in the propagation environment. The persons are modelled by a vertical cylinder of width 40cm and height 170cm. The multi-paths are simulated from reflections on the building vertical partitions (light walls, strong walls, doors, windows and high cupboards), reflections on the ground and ceiling, reflections on the external walls of neighbour buildings, diffractions at the indoor partition edges and diffractions at the neighbour building edges. The attenuation along the different path accounts for the losses due to the transmission through building vertical partitions, floor ground and ceiling.

The simulated radio link is a line-of-sight link into a large room within a corporate building; the AP and MD antenna heights are 1.5m; the simulation frequency is 2GHz. Three different AP locations are tested: AP1 located on a table in the middle of a meeting room (about 33m²); AP2 and AP3 located on a table in the middle of large "open spaces" (around 57m²) as illustrated in Fig. 3.

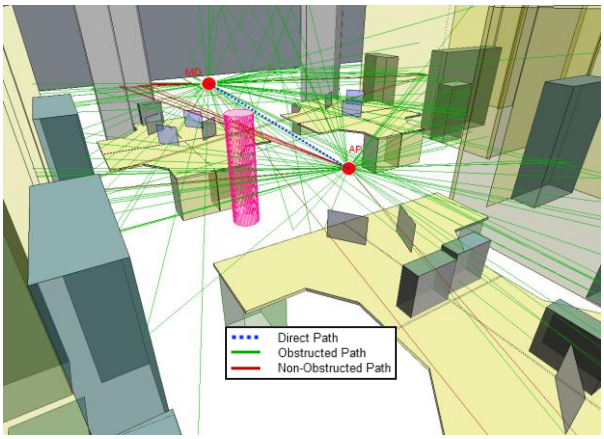

Figure 3. Obstruction probabilities function get from ray-tracing simulation. Human body represented by 3D cylinder (magenta).

Only the paths of interest are kept for the obstruction analysis, i.e. indirect paths with relative power greater than -50dB (relative to the strongest path get at the same MD location). Besides, for simplicity, the analysis has been restricted to paths propagating in nearly the horizontal plane, i.e. without any reflection on floor ground or ceiling. Finally, about 16.6M path-person pairs are generated, for which the obstruction state is determined.

As only the horizontal paths are considered here, the obstruction probability function reduces to:

$$f(\Delta l,dh_1,\phi_1,\ dh_2,\ \phi_2) = 1 - f'(\Delta l,dh_1,\phi_1)\times f'(\Delta l,dh_2,\phi_2) \quad (3)$$

An analytical formulation of $f'(\Delta l,dh_1,\phi_1)$ and $f'(\Delta l,dh_2,\phi_2)$ is derived that matches very well the obstruction probabilities obtained from the ray-tracing: a cross-correlation of 97% is obtained.

Besides, the analysis of transition probabilities has not been completed yet. But a simple approach has been selected based on first observations:

$$g(\Delta l,dh_1,\phi_1,dh_2,\phi_2,S_{I-1,J,K},\delta_{I,J,K}) =$$
$$\xi\times\alpha + f(\Delta l,dh_1,\phi_1,dh_2,\phi_2)\times(1-\alpha) \quad (4)$$

where ξ depends on the obstruction state at the previous snapshot: $\xi = 1$ in case of obstruction; $\xi = 0$ else; and α is a correlation coefficient depending on the distance $\delta_{I,J,K}$ covered by the person PT_J since the last obstruction transition; $\alpha = 1$, when $\delta_{I,J,K} < 40$cm guarantees the obstruction to last at least the whole time used by the person to cover 40cm.

IV. Simulation Results

In the scenario presented in Fig. 4, two persons are moving along different trajectories and cross the LOS direct path at different times. The person velocity is 1m/s and the length of both trajectories is 10m. The narrowband received power variations at 2GHz are predicted considering all two persons together with one snapshot every 1mm movement. Fig. 5 shows that the received power reaches minima when the path is obstructed by one of the person. The fading length and fading amplitude depend on each obstruction situation. Moreover, the received power undergoes significant oscillations (about 2dB amplitude) between two obstructions.

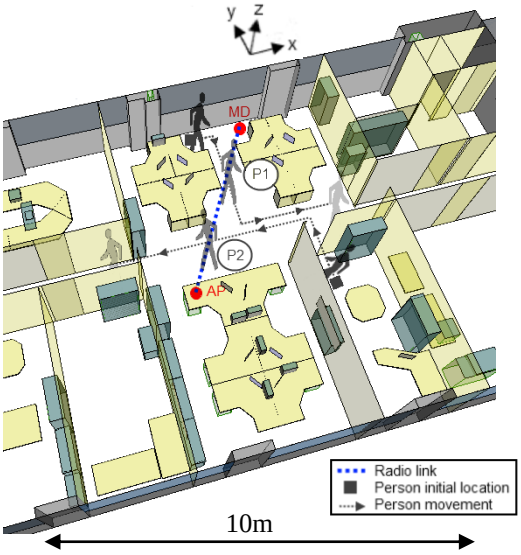

Figure 4. Second simulation scenario.

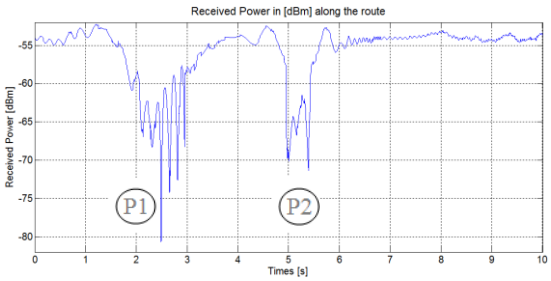

Figure 5. Received power variations from two moving persons

Conclusion

A generic model has been presented for introduction of a time-variant component into stochastic channel models. The purpose is to provide realistic channel realizations for indoor geolocation algorithms, accounting for the human activity impact. Variability studies can therefore be carried out. The model is illustrated at frequency 2GHz in a LOS corporate environment.

Most of the model characteristics rely on previously published results and ray-tracing based obstruction statistics. However, some proposition must still be confirmed (obstruction loss by multiple persons, transition probability function). And the parameterization must be extended to a wider range of configurations.

Acknowledgment

This work has been partly funded by WHERE2 Project (ICT-248894).

References

[1] ITU, *Propagation data and prediction methods for the planning of indoor radiocommunication systems and radio local area networks in the frequency range 900 MHz to 100 GHz*, ITU-R P.1238-6, 2009.

[2] IEEE 802.11, *TGn channel models*, IEEE 802.11-03/940r0, 2003.

[3] WINNER II IST project, *WINNER II channel models - Channel models*, Delivery D1.1.2 part I v1.2, Sept. 2007.

[4] N.J. Thomas, D.J Cruickshank and D.I. Laurenson, "Channel Model Implementation for Evaluation of Location Services", IEE 3G Mobile communication Technologies, Conference Publication No. 47, 2000.

[5] F. Akgul and K.Pahlavan, "A New Ray Optical Statistical Model for Multipath Characteristics Pertinent to Indoor Geolication", IEEE Wireless Communications and Networking Conference (WCNC), Budapest, Hungary, April 2009.

[6] R.J.C. Bultitude, "Measurement, characterization and modelling of indoor 800/900MHz radio channels for digital communications", *IEEE communications magazine*, June 1987.

[7] J. Roberts and J. Abeysinghe, "A two-state Rician Model for Predicting Indoor Wireless Communication Performance", *Proceedings of IEEE International Conference on Communications*, 1995.

[8] M. Varshney, Z. Ji, M. Takai and R. Bagrodia, "Modeling environmental mobility and its effect on network protocol stack", *Proceedings of the IEEE Wireless Communications and Networking Conference (WCNC)*, April 2006.

[9] A. Jraifi, E.H. Saidi, A. El Khafaji and J. el Abbadi, "A temporal variation in indoor environment", *Proceedings of the European computing conference*, 2009.

[10] Y. Lostanlen and Y. Corre, "A propagation prediction method for the study of WLAN indoor environments", *IEEE European Workshop on Integrated Radio-Communication Systems*, Angers, France, May 2002.

REFERENCES

[1] W. Wang, T. Jost, and A. Dammann. Estimation and modelling of nlos time-variant multipath for localization channel model in mobile radios. In *The IEEE Global Communications Conference (GLOBECOM 2010)*, Miami, USA, December 2010.

[2] C. Mensing, S. Sand, A. Dammann, and W.Utschick. Location Estimation in Cellular OFDM Communications Systems. In *IEEE Global Communications Conference (GLOBECOM)*, Honolulu, USA, November/December 2009.

[3] W. Wang, T. Jost, and A. Dammann. Outdoor to Indoor Channel Characteristics on Different Floors. *European Transactions on Telecommunications (ETT)*, 21(5), Aug. 2010.

[4] B. Fleury, M. Tschudin, R. Heddergott, D. Dahlhaus, , and K. Pedersen. Channel Parameter Estimation in Mobile Radio Environments Using the SAGE Algorithm. *IEEE Journal on Selected Areas in Communications*, 17(3):434–450, March 1999.

[5] A. Richter. *Estimation of Radio Channel Parameters: Models and Algorithms*. Ph. D. dissertation, 2005. ISBN: 978-3-938843-02-4.

[6] A. Lehner. *Multipath Channel Modelling for Satellite Navigation Systems*. Ph. D. dissertation, 2007. ISBN: 978-3-8322-6651-6.

[7] Jussi Salmi, Andreas Richter, and Visa Koivunen. Detection and tracking of MIMO propagation path parameters using state-space approach. *IEEE Transactions on Signal Processing*, 57(4):1538–1550, Apr. 2009.

[8] W. Wang and T. Jost. Evaluation of time-variant multipath characteristics for localization channel model in terrestrial mobile radio. In *COST Action IC0802, Propagation tools and data for integrated Telecommunication, Navigation and Earth Observation systems. MCM 3*, Athens, Greece, April 2010.

[9] M. Varshney, Z. Ji, M. Takai, and R. Bagrodia. Modeling environmental mobility and its effect on network protocol stack. In *Proc. IEEE Wireless Communications and Networking Conference (WCNC)*, Las Vegas, NV, USA, April 2006.

[10] Mohammed Khider, Susanne Kaiser, Patrick Robertson, and Michael Angermann. A novel movement model for pedestrians suitable for personal navigation. In *Proceedings of ION NTM Conference 2008*, 2008.

[11] Dirk Helbing and Péter Molnár. Social force model for pedestrian dynamics. *Phys. Rev. E*, 51(5):4282–4286, May 1995.

[12] Philip J. DiNenno, editor. *SFPE Handbook of Fire Protection Engineering*. National Fire Protection Association, 2002.

[13] Dirk Helbing, Joachim Keltsch, and Peter Molnar. Modelling the evolution of human trail systems. *Nature*, 388:47–50, 1997.